

# Electro-mechanical singularities of piezoelectric bi-materials and interface cracks

M. Hrstka<sup>a,\*</sup>, T. Profant<sup>a</sup>, M. Kotoul<sup>a</sup>

<sup>a</sup>*Institute of Solid Mechanics, Mechatronics and Biomechanics, Brno University of Technology; Technická 2896/2, 616 69 Brno, Czech Republic*

---

## Abstract

The complex potentials constitute the Lekhnitskii-Eshelby-Stroh formalism and its extension form is used to grasp the particular properties and behaviour of the piezoelectric bi-material notch and interface crack. The material inhomogeneity and piezoelectricity supplement the stress singularity with further electric one and make the stress and electric field at the concentrator tip more complicated. The application of the Lekhnitskii-Eshelby-Stroh formalism to the prevailing boundary conditions at the concentrator tip leads to the solution of the stress and electric displacement exponent eigenvalue problem, whose results are analysed. The evaluated eigenvectors substituted to the complex potentials form the regular and auxiliary solutions which are the basis of the singular and dual part of the stress field as well as the electrical field at the concentrator tip. The orthogonality between the regular and auxiliary solutions is applied via the  $\Psi$ -integral to the numerical FEM solution to evaluate the generalized stress intensity factors.

**Keywords:** Extended Lekhnitskii-Eshelby-Stroh formalism, piezoelectricity, bi-material notch, interface crack,  $\Psi$ -integral, generalized stress intensity factor

---

## 1. Introduction

Piezoelectric material is extensively used as sensors or actuators in intelligence advanced structure design, as well as in many branches of science. It is well known that piezoelectric materials produce an electric field when deformed  
5 and undergo deformation when subjected to an electric field. This is so-called intrinsic electro-mechanical coupling phenomenon. Commonly used piezoelectric materials are ceramics manufactured by conventional ceramic processing. In order to insure the reliability and structural integrity of electro-mechanical devices using these materials, it is necessary to understand their mechanical

---

\*Corresponding author  
Email address: ? (M. Hrstka)

10 behaviour. There have been many researches dealing with behaviour of piezo-  
electric ceramics.

Solutions presented in [1], [2], [3], [4], [5], [6] show that equations for piezo-  
electric anisotropic problem have same structure as those for corresponding  
anisotropic elastic materials. Closed form solution of a central crack based on  
15 expanded Stroh formalism was derived in [5], while solution for elliptic inclusion  
and hole was done in [7], [6], [8]. First attempt to express material matrices  
explicitly was done in [9]. The most significant work was done by Hwu in [10],  
[11], [12], [13] and also in his monograph [14], where he summed up the previous  
research and extended the Stroh formalism, his Key matrix and the unified defi-  
20 nition [15] to the piezoelectric media. Hirai et al. [16] and Abe et al. [17] applied  
the theory to certain bi-material notch configuration including determination of  
stress intensity factors by  $\Psi$ -integral method.

Similar progress had been done for expanding the Lekhnitskii formalism in  
[18], [19]. General solution for piezoelectric anisotropic material was derived  
25 in [20], [21], [22], [23], [24], [25]. Xu and Rajapakse [26], Chue and Chen [27]  
or Chen [28] investigated composite piezoelectric wedges and junctions, i.e. bi-  
materials composed from both piezoelectric and anisotropic materials. Stress  
intensity factors of an interface crack in isotropic metal/piezoelectric ceramics  
were computed in [29], [30] or in [31] for an interface between anisotropic/pie-  
30 zoelectric materials. Banks-Sills et al. [32] calculated stress intensity factors by  
M-integral method.

The anisotropy of the piezoelectric materials require the corresponding math-  
ematical tools to handle with their behaviour. The piezoelectric continuum is  
governed by the expanded equations of linear electromechanical statics. Ac-  
35 cording to this state, the extended Stroh formalism has been developed by Hwu  
[10, 13, 11].

Suo [33] developed the Lekhnitskii-Eshelby-Stroh formalism (LES formal-  
ism) for evaluating the stress singularity of an anisotropic bi-material notches.  
However, its limit case - an interface crack - is primarily treated as the Hilbert  
40 problem, as can be seen in [6], [34], [35], [36], [37], [38], [39]. The present work  
applies the extended LES formalism for piezoelectric continuum based on the  
studies [40, 14, 41] and applies it to the problem of piezoelectric bi-material  
notch and interface crack. In addition, both singular concentrator types are  
involved into one procedure that do not distinguish whether the value of the  
45 stress singularity exponent is complex or real, respectively.

In the literature there is a gap in investigation of the notches whose value  
of the stress singularity exponent becomes complex. This state can occur when  
e.g. a de-laminated interface has face angles very close to an interface crack. In  
the following paragraphs it is to be shown that the LES formalism presented  
50 in previously stated papers can be applied through the problems of the notch  
geometry showing oscillatory index to the problems of the interface cracks as its  
limit case. Even that the developed particular stress and displacement equations  
have a slightly different form as usually appeared in [33], the resulting stress  
and displacement development are equal. First, the theory for anisotropic bi-  
55 material has to be investigated in order to get its limit of application, then its

expansion to the LES formalism for piezoelectric material is provided.

## 2. Constitutive laws for piezoelectric materials

There are natural crystals such as quartz that exhibit piezoelectricity. Much more stronger piezoelectric coupling exhibit man-made piezoelectric materials, e.g. barium titanate or lead zirconate ceramics. These materials are implicitly in isotropic and non-piezoelectric state. Piezoelectric properties can be induced in these ceramics through a so-called poling process [42], during which their above mentioned mechanical properties change to generally anisotropic. However, most poled materials become transversally isotropic.

Material characteristics of piezoelectric materials are predominantly provided by elastic stiffnesses  $C_{ij}^E$ , piezoelectric constants  $e_{ij}$  and dielectric permittivities  $\omega_{ij}^\varepsilon$ . The stiffness, piezoelectric and permittivity matrices  $\mathbf{C}_E$ ,  $\mathbf{e}$  and  $\boldsymbol{\omega}_\varepsilon$  characterise the most general form of an anisotropic material with piezoelectric properties. The symmetry planes will coincide with the global coordinate planes in the Cartesian coordinate system  $x_1, x_2, x_3$ .

As it is stated above, the initially isotropic ceramic becomes transversally isotropic during the poling process with the plane of isotropy parallel to the poling axis. The transversally isotropic state of the material is the most important one in the study of poled piezoelectric materials, but it is a special case of the more general monoclinic material whose elasticity and piezoelectricity matrices have the following structure:

$$\mathbf{C}_E = \begin{bmatrix} C_{11}^E & C_{12}^E & C_{13}^E & 0 & 0 & C_{16}^E \\ C_{12}^E & C_{22}^E & C_{23}^E & 0 & 0 & C_{26}^E \\ C_{13}^E & C_{23}^E & C_{33}^E & 0 & 0 & C_{36}^E \\ 0 & 0 & 0 & C_{44}^E & C_{45}^E & 0 \\ 0 & 0 & 0 & C_{45}^E & C_{55}^E & 0 \\ C_{16}^E & C_{26}^E & C_{36}^E & 0 & 0 & C_{66}^E \end{bmatrix}, \quad (1)$$

$$\mathbf{e} = \begin{bmatrix} e_{11} & e_{12} & e_{13} & 0 & 0 & e_{16} \\ e_{21} & e_{22} & e_{23} & 0 & 0 & e_{26} \\ 0 & 0 & 0 & e_{34} & e_{35} & 0 \end{bmatrix}, \quad \boldsymbol{\omega}_\varepsilon = \begin{bmatrix} \omega_{11}^\varepsilon & \omega_{12}^\varepsilon & 0 \\ \omega_{12}^\varepsilon & \omega_{22}^\varepsilon & 0 \\ 0 & 0 & \omega_{33}^\varepsilon \end{bmatrix}.$$

It is worth noticing that the stiffness and permittivity matrices are symmetric, but the piezoelectric matrix is not. The directional properties of the matrices depend on the poling axis. The structure of the piezoelectric matrix depends on the poling directions, which can attain two limit configurations: coincidence with  $x_1$ -axis or with  $x_2$ -axis. Between these states their structure corresponds to the above mentioned monoclinic one. It is illustrated in the following scheme:

$$\begin{aligned}
& \parallel x_1 \begin{bmatrix} e_{11} & e_{12} & e_{12} & 0 & 0 & 0 \\ 0 & 0 & 0 & 0 & 0 & e_{26} \\ 0 & 0 & 0 & 0 & e_{26} & 0 \end{bmatrix} \\
& \Downarrow \\
& \text{in between} \begin{bmatrix} e_{11} & e_{12} & e_{13} & 0 & 0 & e_{16} \\ e_{21} & e_{22} & e_{23} & 0 & 0 & e_{26} \\ 0 & 0 & 0 & e_{34} & e_{35} & 0 \end{bmatrix} \\
& \Downarrow \\
& \parallel x_2 \begin{bmatrix} 0 & 0 & 0 & 0 & 0 & e_{16} \\ e_{21} & e_{22} & e_{21} & 0 & 0 & 0 \\ 0 & 0 & 0 & e_{16} & 0 & 0 \end{bmatrix}
\end{aligned} \tag{2}$$

75 In the further paragraphs we consider a monoclinic or transversally isotropic materials only, because allow one to decouple a solved problem to an in-plane and anti-plane. When the material specimen is loaded in the  $x_1x_2$  plane, we can focus only on the in-plane problem, where the singularity is significant according to loading state.

Let us consider rotation of the material coordinate system about  $x_3$  axis by an angle of  $90^\circ$  and  $-90^\circ$ , i.e. we coincide the poling direction with  $x_2$  axis. Then the resulting stiffness matrix of the considered piezoelectric monoclinic material does not change, on the other hand the elements of the piezoelectric matrix change the sign. The structure of the permittivity matrices remains unchanged. From this follows that the poling has unique orientation and contrary to the adopted laminate theory there are no symmetries in rotations of the longitudinal directions. More about matrix structure of individual crystal classes can be found in [43, p. 123].

80 For an anisotropic and linearly electro-elastic solid, the constitutive laws between elastic field tensors ( stresses  $\sigma_{ij}$  and deformations  $\varepsilon_{ij}$ ) and electric field vectors (electric displacements  $D_j$  and electric field  $E_j$ ) are represented by four equally important equation systems. Using the contracted notation, the constitutive laws can be then written in a matrix form as [10]

$$\begin{aligned}
\begin{Bmatrix} \sigma \\ \mathbf{D} \end{Bmatrix} &= \begin{bmatrix} \mathbf{C}_E & \mathbf{e}^\top \\ \mathbf{e} & -\omega_\varepsilon \end{bmatrix} \begin{Bmatrix} \varepsilon \\ -\mathbf{E} \end{Bmatrix}, \quad \begin{Bmatrix} \varepsilon \\ \mathbf{D} \end{Bmatrix} = \begin{bmatrix} \mathbf{S}_E & -\mathbf{d}^\top \\ \mathbf{d} & -\omega_\sigma \end{bmatrix} \begin{Bmatrix} \sigma \\ -\mathbf{E} \end{Bmatrix}, \\
\begin{Bmatrix} \sigma \\ -\mathbf{E} \end{Bmatrix} &= \begin{bmatrix} \mathbf{C}_D & -\mathbf{h}^\top \\ \mathbf{h} & -\beta_\varepsilon \end{bmatrix} \begin{Bmatrix} \varepsilon \\ \mathbf{D} \end{Bmatrix}, \quad \begin{Bmatrix} \varepsilon \\ -\mathbf{E} \end{Bmatrix} = \begin{bmatrix} \mathbf{S}_D & \mathbf{g}^\top \\ \mathbf{g} & -\beta_\sigma \end{bmatrix} \begin{Bmatrix} \sigma \\ \mathbf{D} \end{Bmatrix},
\end{aligned} \tag{3}$$

where

$$\begin{aligned} \boldsymbol{\sigma} = \begin{Bmatrix} \sigma_1 \\ \sigma_2 \\ \sigma_3 \\ \sigma_4 \\ \sigma_5 \\ \sigma_6 \end{Bmatrix} &= \begin{Bmatrix} \sigma_{11} \\ \sigma_{22} \\ \sigma_{33} \\ \sigma_{23} \\ \sigma_{13} \\ \sigma_{12} \end{Bmatrix}, \quad \boldsymbol{\varepsilon} = \begin{Bmatrix} \varepsilon_1 \\ \varepsilon_2 \\ \varepsilon_3 \\ \varepsilon_4 \\ \varepsilon_5 \\ \varepsilon_6 \end{Bmatrix} = \begin{Bmatrix} \varepsilon_{11} \\ \varepsilon_{22} \\ \varepsilon_{33} \\ 2\varepsilon_{23} \\ 2\varepsilon_{13} \\ 2\varepsilon_{12} \end{Bmatrix}, \\ \mathbf{E} &= \begin{Bmatrix} E_1 \\ E_2 \\ E_3 \end{Bmatrix}, \quad \mathbf{D} = \begin{Bmatrix} D_1 \\ D_2 \\ D_3 \end{Bmatrix}, \end{aligned} \quad (4)$$

The superscript  $\mathsf{T}$  denotes matrix transposition. Expressions for matrices  $\mathbf{S}_E$ ,  $\mathbf{S}_D$ ,  $\mathbf{C}_D$ ,  $\mathbf{d}$ ,  $\mathbf{g}$ ,  $\mathbf{h}$ ,  $\boldsymbol{\omega}_\sigma$ ,  $\boldsymbol{\beta}_\sigma$  and  $\boldsymbol{\beta}_\varepsilon$  can be evaluated from the relations

$$\begin{bmatrix} \mathbf{C}_E & \mathbf{e}^\mathsf{T} \\ \mathbf{e} & -\boldsymbol{\omega}_\varepsilon \end{bmatrix} \begin{bmatrix} \mathbf{S}_D & \mathbf{g}^\mathsf{T} \\ \mathbf{g} & -\boldsymbol{\beta}_\sigma \end{bmatrix} = \mathbf{I}, \quad \begin{bmatrix} \mathbf{C}_D & -\mathbf{h}^\mathsf{T} \\ \mathbf{h} & -\boldsymbol{\beta}_\varepsilon \end{bmatrix} \begin{bmatrix} \mathbf{S}_E & -\mathbf{d}^\mathsf{T} \\ \mathbf{d} & -\boldsymbol{\omega}_\sigma \end{bmatrix} = \mathbf{I}, \quad (5)$$

where the matrix  $\mathbf{I}$  is the unit matrix of a shape  $9 \times 9$ . In order to investigate material configurations in an arbitrary poling axis orientation in the plane  $x_3 = 0$ , transformation relations have to be defined. Let us designate the principal material coordinate system  $x_i^*$ , in which we assemble the stiffness, piezoelectric and permittivity matrices and perform their inverse by (5) to obtain compliance matrix  $\mathbf{S}_D^*$ , piezoelectric matrix  $\mathbf{g}^*$  and non-permittivities<sup>1</sup>  $\boldsymbol{\beta}_\sigma^*$ . Then we can transform the compliance matrix of the piezoelectric material as follows

$$\mathbf{S}_D = (\mathbf{K}^{-1})^\mathsf{T} \mathbf{S}_D^* \mathbf{K}^{-1}, \quad \mathbf{g} = \boldsymbol{\Omega} \mathbf{g}^* \mathbf{K}^{-1}, \quad \boldsymbol{\beta}_\sigma = \boldsymbol{\Omega} \boldsymbol{\beta}_\sigma^* \boldsymbol{\Omega}^{-1}, \quad (6)$$

where the transformation matrices  $\mathbf{K}$  and  $\boldsymbol{\Omega}$  are defined by

$$\mathbf{K} = \begin{bmatrix} \cos^2 \alpha & \sin^2 \alpha & 0 & 0 & 0 & 2 \cos \alpha \sin \alpha \\ \sin^2 \alpha & \cos^2 \alpha & 0 & 0 & 0 & -2 \cos \alpha \sin \alpha \\ 0 & 0 & 1 & 0 & 0 & 0 \\ 0 & 0 & 0 & \cos \alpha & -\sin \alpha & 0 \\ 0 & 0 & 0 & \sin \alpha & \cos \alpha & 0 \\ -\cos \alpha \sin \alpha & \cos \alpha \sin \alpha & 0 & 0 & 0 & \cos^2 \alpha - \sin^2 \alpha \end{bmatrix}, \quad (7)$$

$$\boldsymbol{\Omega} = \begin{bmatrix} \cos \alpha & \sin \alpha & 0 \\ -\sin \alpha & \cos \alpha & 0 \\ 0 & 0 & 1 \end{bmatrix}. \quad (8)$$

<sup>85</sup> The angle  $\alpha$  defines a rotation about  $x_3$  axis in counter-clockwise direction and physically means the poling direction of the material. With respect to the material symmetry, the monoclinic materials with the symmetry axis parallel to

---

<sup>1</sup>Dielectric permittivity has not an inverse quantity. In some papers it is stated that the inverse is electric susceptibility  $\chi_e$ , but these parameters are not inverse, but it is  $\chi_e = \omega_\varepsilon - 1$ . Owing to this fact, we adopted the Hwu's non-permittivity [10].

$x_3 = 0$  is to be considered. It is the most general material configuration when the extended LES formalism can be employed. The stress and displacement  
 90 relations in the  $x_3$  direction are the functions of the  $x_1$  and  $x_2$  coordinates only in this materials. The in-plane and anti-plane fields can be decoupled and hence the solved problem could be rather simplified. Under the assumption that external loads are parallel to a plane defined by  $x_3 = 0$ , we can focus on the in-plane field only. Note that anti-plane stresses or strains are not zero (with taking  
 95 individual plane deformation state into the consideration), but their effects are induced by the in-plane loads and one can claim that their influence is less significant from the in-plane loading point of view. More detailed studies of the anti-plane fields were published in [44], [45], [27] [46], [47], [48] and [49].

Except the reduction of the independent variables to  $x_1$  and  $x_2$ , an important simplification in the decoupling of the plane fields is the rank reduction of the matrices (1) of the constitutive laws, which can be written as

$$\begin{Bmatrix} \boldsymbol{\sigma} \\ \mathbf{D} \end{Bmatrix} = \begin{bmatrix} \hat{\mathbf{C}}'_E & \hat{\mathbf{e}}'^T \\ \hat{\mathbf{e}}' & -\hat{\boldsymbol{\omega}}'_\varepsilon \end{bmatrix} \begin{Bmatrix} \boldsymbol{\varepsilon} \\ -\mathbf{E} \end{Bmatrix}, \quad \begin{Bmatrix} \boldsymbol{\varepsilon} \\ -\mathbf{E} \end{Bmatrix} = \begin{bmatrix} \hat{\mathbf{S}}'_D & \hat{\mathbf{g}}'^T \\ \hat{\mathbf{g}}' & -\hat{\boldsymbol{\beta}}'_\sigma \end{bmatrix} \begin{Bmatrix} \boldsymbol{\sigma} \\ \mathbf{D} \end{Bmatrix}, \quad (9)$$

where

$$\boldsymbol{\sigma} = \begin{Bmatrix} \sigma_1 \\ \sigma_2 \\ \sigma_6 \end{Bmatrix}, \quad \boldsymbol{\varepsilon} = \begin{Bmatrix} \varepsilon_1 \\ \varepsilon_2 \\ \varepsilon_6 \end{Bmatrix}, \quad \mathbf{E} = \begin{Bmatrix} E_1 \\ E_2 \end{Bmatrix}, \quad \mathbf{D} = \begin{Bmatrix} D_1 \\ D_2 \end{Bmatrix} \quad (10)$$

and

$$\hat{\mathbf{C}}'_E = \begin{bmatrix} \hat{C}'_{11} & \hat{C}'_{12} & \hat{C}'_{16} \\ \hat{C}'_{12} & \hat{C}'_{22} & \hat{C}'_{26} \\ \hat{C}'_{16} & \hat{C}'_{26} & \hat{C}'_{66} \end{bmatrix}, \quad \hat{\mathbf{e}}' = \begin{bmatrix} \hat{e}'_{11} & \hat{e}'_{12} & \hat{e}'_{16} \\ \hat{e}'_{21} & \hat{e}'_{22} & \hat{e}'_{26} \end{bmatrix}, \quad \hat{\boldsymbol{\omega}}'_\varepsilon = \begin{bmatrix} \hat{\omega}'_{11} & \hat{\omega}'_{12} \\ \hat{\omega}'_{21} & \hat{\omega}'_{22} \end{bmatrix}. \quad (11)$$

$$\hat{\mathbf{S}}'_D = \begin{bmatrix} \hat{S}'_{11} & \hat{S}'_{12} & \hat{S}'_{16} \\ \hat{S}'_{12} & \hat{S}'_{22} & \hat{S}'_{26} \\ \hat{S}'_{16} & \hat{S}'_{26} & \hat{S}'_{66} \end{bmatrix}, \quad \hat{\mathbf{g}}' = \begin{bmatrix} \hat{g}'_{11} & \hat{g}'_{12} & \hat{g}'_{16} \\ \hat{g}'_{21} & \hat{g}'_{22} & \hat{g}'_{26} \end{bmatrix}, \quad \hat{\boldsymbol{\beta}}'_\sigma = \begin{bmatrix} \hat{\beta}'_{11} & \hat{\beta}'_{12} \\ \hat{\beta}'_{12} & \hat{\beta}'_{22} \end{bmatrix} \quad (12)$$

The constitutive laws (9) are the in-plane part of the generalized plain strain and short circuit form of the first and last constitutive law in (3) also known as e-type and g-type, respectively. The reduced elements of the matrices in (9) are evaluated from the matrices in (3) under the assumption that  $\varepsilon_3 = 0$  and  $E_3 = 0$ . This leads to the expressions

$$\hat{C}'_{ij} = C_{ij}^E, \quad \hat{e}'_{ij} = e_{ij}, \quad \hat{\omega}'_{ij} \varepsilon = \omega_{ij}^\varepsilon, \quad (13)$$

$$\hat{S}'_{ij} = \hat{S}_{ij}^D + \frac{\hat{g}_{3i} \hat{g}_{3j}}{\hat{\beta}_{33}^\sigma} = \hat{S}_{ji}^D, \quad \hat{g}'_{ij} = \hat{g}_{ij} - \frac{\hat{\beta}_{3i}^\sigma \hat{g}_{3j}}{\hat{\beta}_{33}^\sigma}, \quad \hat{\beta}'_{ij} = \hat{\beta}_{ij}^\sigma - \frac{\hat{\beta}_{3i}^\sigma \hat{\beta}_{3j}^\sigma}{\hat{\beta}_{33}^\sigma} = \hat{\beta}_{ji}^\sigma, \quad (14)$$

in which

$$\hat{S}_{ij}^D = S_{ij}^D - \frac{S_{3i}^D S_{3j}^D}{S_{33}^D} = \hat{S}_{ji}^D, \quad \hat{g}_{ij} = g_{ij} - \frac{g_{i3} S_{3j}^D}{S_{33}^D}, \quad \hat{\beta}_{ij}^\sigma = \beta_{ij}^\sigma + \frac{g_{i3} g_{j3}}{S_{33}^D} = \hat{\beta}_{ji}^\sigma \quad (15)$$

for  $i, j \neq 3$ . There are more plane generalisations of the piezoelectricity, see [10], which are not discussed here.

### 3. Weak formulation of piezoelectric problem under generalized plane considerations

The virtual work and the energy-based formulation is established from the governing equations of the electrostatic behaviour of the piezoelectric continua. In the absence of the body forces and free charges, the equilibrium equations are

$$\frac{\partial \sigma_{ij}}{\partial x_j} = 0, \quad \frac{\partial D_i}{\partial x_i} = 0, \quad (16)$$

where repeated indices imply the summation. The strain tensor  $\boldsymbol{\varepsilon}$  and the electric field vector  $\mathbf{E}$  are linked to displacements  $\mathbf{u}$  and the electric potential  $\phi$  by the relations

$$\varepsilon_{ij} = \frac{1}{2} \left( \frac{\partial u_i}{\partial x_j} + \frac{\partial u_j}{\partial x_i} \right), \quad E_i = -\frac{\partial \phi}{\partial x_i}. \quad (17)$$

The character of the boundary conditions under which the piezoelectric body  $\Omega$  is subjected on its boundary  $\partial\Omega$  are mechanical and electric. The Dirichlet boundary conditions are

$$\mathbf{u} = \bar{\mathbf{u}} \quad \text{and} \quad \phi = \bar{\phi} \quad (18)$$

and the Neumann ones

$$t_i = \sigma_{ij} n_j \quad \text{and} \quad D_i n_i = -q, \quad (19)$$

where

$$q = \frac{1}{4\pi} \frac{\partial E_i}{\partial x_i}. \quad (20)$$

is the surface charge and  $\mathbf{n}$  is the unit outward normal to the surface  $\partial\Omega$ . The repeated indices means again the summation as well as in the following weak formulation. For arbitrary virtual displacement  $\delta\mathbf{u}$  and electrical potential  $\delta\phi$  the weak form of the problem given by the equations (16) can be written as, see e.g. [50],

$$-\int_{\Omega} \sigma_{ij} \delta \varepsilon_{ij} d\Omega + \int_{\Omega} D_i \delta E_i d\Omega + \int_{\partial\Omega} t_i \delta u_i d\partial\Omega - \int_{\partial\Omega} q \delta \phi d\partial\Omega = 0. \quad (21)$$

Substituting the constitutive law (9)<sub>1</sub> into (21) leads to the electric potential variational principle as the starting point of the so-called mixed finite element

105 formulation using the variables  $\mathbf{u}$  and  $\phi$ . The results received from the finite  
 element analysis is the necessary input into the generalized stress intensity fac-  
 tor evaluation of the bi-material stress concentrator described in the following  
 paragraphs. More about the mixed finite element method can be found in e.g.  
 [51], [52]. The script for the finite element computing platform FEniCS 2018.1  
 110 is given in Appendix A.

#### 4. Stress singularity of piezoelectric bi-material notch and interface crack

Similarly to the pure anisotropic elasticity, present research of piezoelectric  
 bi-material singular concentrators is reduced to such cases when principal mate-  
 115 rial directions of transversally isotropic piezoelectric materials are in coincidence  
 with global Cartesian axes. This brings about simplifications of governing equa-  
 tions.

A poled piezoelectric ceramic has different material characteristics in the  
 poling direction than in the perpendicular plane, in which the material be-  
 120 haviour is isotropic. Similarly as by pure anisotropic elasticity, the character-  
 istic matrices of the material are non-degenerate when the poling direction is  
 perpendicular with the  $x_3$  axis and semi-degenerate or degenerate otherwise.  
 The non-degenerate materials only are discussed in the following text, because  
 the semi-degenerate and degenerate materials require special treatment, see [14,  
 125 p. 385].

We focus on the technical types of non-degenerate materials with hexagonal  
 crystals. Typical representatives are lead zirconate titanate - PZT-4, PZT-5H,  
 PZT-6B, PZT-7, PZT-7A, barium titanate  $\text{BaTiO}_3$ , or zinc oxide  $\text{ZnO}$ . These  
 functional ceramics possess the actuating strain (maximal to 0.2%), the high  
 130 stiffness and the high response. In that cases the in-plane and anti-plane fields  
 can be decoupled when proper orientations are considered.

The extended LES formalism for piezoelectric media is an power analytical  
 tool, which can solve the problems of the bi-material notches composed of the  
 monoclinic materials. The stress singularity at the notch composed of the two  
 monoclinic piezoelectric materials and solved as the in-plane problem is charac-  
 terized by two complex exponents  $\delta_1 - 1$ ,  $\delta_2 - 1$  and one real exponent  $\delta_3 - 1$ .  
 The resulting displacements and stresses are obtained as the superposition of  
 these particular singular contributions weighted by the generally complex am-  
 plitudes. The amplitudes are introduced in the similar manner as well as for a  
 crack and generalized to the case of the sharp notch as the generalized stress  
 intensity factors (GSIFs). In the first we introduce the vectors

$$\mathbf{u} = \begin{Bmatrix} u_1 \\ u_2 \\ \phi \end{Bmatrix}, \quad \mathbf{T} = \begin{Bmatrix} T_1 \\ T_2 \\ T_D \end{Bmatrix}, \quad (22)$$

where  $\phi$  is the above defined electric potential,  $T_1$ ,  $T_2$  and  $T_D$  are the components  
 of the resulting tractions and the electric charge  $q$  along the semi-infinity line



situated at the origin of the coordinate system  $x_1x_2$ . Then the vectors  $\mathbf{u}$  and  $\mathbf{T}$  at the tip of a piezoelectric bi-material wedge has the form [41]

$$\begin{aligned}\mathbf{u}(r, \theta) &= H_1 r^{\delta_1} \boldsymbol{\eta}_1(\theta) + H_2 r^{\delta_2} \boldsymbol{\eta}_2(\theta) + H_3 r^{\delta_3} \boldsymbol{\eta}_3(\theta), \\ \mathbf{T}(r, \theta) &= H_1 r^{\delta_1} \boldsymbol{\lambda}_1(\theta) + H_2 r^{\delta_2} \boldsymbol{\lambda}_2(\theta) + H_3 r^{\delta_3} \boldsymbol{\lambda}_3(\theta),\end{aligned}\quad (23)$$

where  $H_i$  are generalized stress intensity factors,  $r$  and  $\theta$  are polar coordinates, see Fig. 1, and

$$\begin{aligned}\boldsymbol{\eta}_i(\theta) &= \mathbf{A} \mathbf{Z}^{\delta_i}(\theta) \mathbf{v}_i + \overline{\mathbf{A}} \overline{\mathbf{Z}}^{\delta_i}(\theta) \mathbf{w}_i, \\ \boldsymbol{\lambda}_i(\theta) &= \mathbf{L} \mathbf{Z}^{\delta_i}(\theta) \mathbf{v}_i + \overline{\mathbf{L}} \overline{\mathbf{Z}}^{\delta_i}(\theta) \mathbf{w}_i.\end{aligned}\quad (24)$$

The matrices  $\mathbf{Z}^{\delta_i}(\theta)$  represent the exponentials of the points in the so-called  $z$ -plane, see [40], corresponding to the points on the unit circle in the  $(x_1, x_2)$ -plane, which can be written as

$$\begin{aligned}\mathbf{Z}^{\delta_i}(\theta) &= \text{diag} \left[ R_1^{\delta_i}(\theta) e^{i\delta_i \Psi_1(\theta)}, R_2^{\delta_i}(\theta) e^{i\delta_i \Psi_2(\theta)}, R_3^{\delta_i}(\theta) e^{i\delta_i \Psi_3(\theta)} \right], \\ \overline{\mathbf{Z}}^{\delta_i}(\theta) &= \text{diag} \left[ R_1^{\delta_i}(\theta) e^{-i\delta_i \Psi_1(\theta)}, R_2^{\delta_i}(\theta) e^{-i\delta_i \Psi_2(\theta)}, R_3^{\delta_i}(\theta) e^{-i\delta_i \Psi_3(\theta)} \right].\end{aligned}\quad (25)$$

where

$$R_k^2(\theta) = (\cos \theta + \mu'_k \sin \theta)^2 + (\mu''_k \sin \theta)^2, \quad (k = 1, 2, 3) \quad (26)$$

$$\Psi_k(\theta) = \begin{cases} \arctan \left( \frac{\mu''_k \sin \theta}{\cos \theta + \mu'_k \sin \theta} \right) & \text{for } \theta > -\pi \\ -\pi & \text{for } \theta = -\pi \end{cases}, \quad (k = 1, 2, 3) \quad (27)$$

The symbols  $\mu'_k$ ,  $\mu''_k$  are real and imaginary part of the material eigenvalue  $\mu_k$ , which is the root of the following characteristic equation

$$l_2(\mu) [l_4(\mu) \rho_2(\mu) - m_3^2(\mu)] = 0, \quad (28)$$

where

$$\begin{aligned}l_2(\mu) &= \hat{S}_{55}'^D \mu^2 - 2\hat{S}_{45}'^D \mu + \hat{S}_{44}'^D, \\ l_4(\mu) &= \hat{S}_{11}'^D \mu^4 - 2\hat{S}_{16}'^D \mu^3 + (2\hat{S}_{12}'^D + \hat{S}_{66}'^D) \mu^2 - 2\hat{S}_{26}'^D \mu + \hat{S}_{22}'^D, \\ m_3(\mu) &= \hat{g}_{11}' \mu^3 - (\hat{g}_{21}' + \hat{g}_{16}') \mu^2 + (\hat{g}_{12}' + \hat{g}_{26}') \mu - \hat{g}_{22}', \\ \rho_2(\mu) &= -\hat{\beta}_{11}'^{\sigma} \mu^2 + 2\hat{\beta}_{12}'^{\sigma} \mu - \hat{\beta}_{22}'^{\sigma}.\end{aligned}\quad (29)$$

The expression in square brackets in (28) gives three material eigenvalues  $\mu_1$ ,  $\mu_2$ ,  $\mu_3$  corresponding to the in-plane solution. There is also eigenvalue  $\mu_4$  as the solution of the anti-plane characteristic equation  $l_2(\mu) = 0$  in (28), which is not taken into account. Remaining matrices in (24) read

$$\mathbf{A} = \begin{bmatrix} a_{11} & a_{12} & a_{14} \\ a_{21} & a_{22} & a_{24} \\ a_{41} & a_{42} & a_{44} \end{bmatrix}, \quad \mathbf{L} = \begin{bmatrix} -\mu_1 & -\mu_2 & -\mu_4 \xi_4 \\ 1 & 1 & \xi_4 \\ -\xi_1 & -\xi_2 & -1 \end{bmatrix}, \quad (30)$$

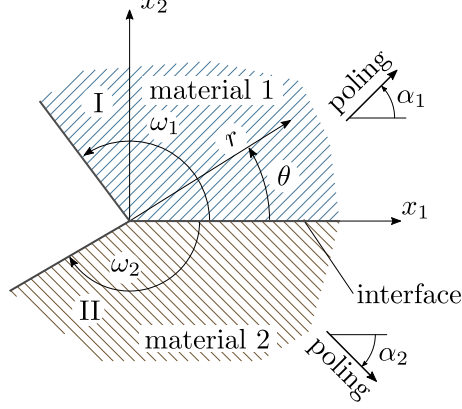


Figure 1: Geometry of a bi-material notch characterized by two regions I and II. Notch faces are defined by angles  $\omega_1$  and  $\omega_2$ . Material interface is always considered at  $\theta = 0$ . Angles  $\alpha_1$  and  $\alpha_2$  denote poling direction of the materials I and II, respectively.

where the elements of the matrices  $\mathbf{A}$  and  $\mathbf{L}$  are defined as ([19], [22], [25], [27], [32])

$$\begin{aligned}
a_{1k} &= \mu_k^2 \hat{S}_{11}'^D + \hat{S}_{12}'^D - \mu_k \hat{S}_{16}'^D + \xi_k (\mu_k \hat{g}_{11}' - \hat{g}_{21}'), \quad (k = 1, 2) \\
a_{2k} &= \left[ \mu_k^2 \hat{S}_{12}'^D + \hat{S}_{22}'^D - \mu_k \hat{S}_{26}'^D + \xi_k (\mu_k \hat{g}_{12}' - \hat{g}_{22}') \right] / \mu_k, \quad (k = 1, 2) \\
a_{4k} &= \left[ \mu_k^2 \hat{g}_{21}' + \hat{g}_{22}' - \mu_k \hat{g}_{26}' + \xi_k (-\mu_k \hat{\beta}_{12}'^{\sigma} + \hat{\beta}_{22}'^{\sigma}) \right] / \mu_k, \quad (k = 1, 2) \\
a_{14} &= \left( \mu_4^2 \hat{S}_{11}'^D + \hat{S}_{12}'^D - \mu_4 \hat{S}_{16}'^D \right) \xi_4 + \mu_4 \hat{g}_{11}' - \hat{g}_{21}', \\
a_{24} &= \left[ \left( \mu_4^2 \hat{S}_{12}'^D + \hat{S}_{22}'^D - \mu_4 \hat{S}_{26}'^D \right) \xi_4 + \mu_4 \hat{g}_{12}' - \hat{g}_{22}' \right] / \mu_4, \\
a_{44} &= \left[ \left( \mu_4^2 \hat{g}_{21}' + \hat{g}_{22}' - \mu_4 \hat{g}_{26}' \right) \xi_4 - \mu_4 \hat{\beta}_{12}'^{\sigma} + \hat{\beta}_{22}'^{\sigma} \right] / \mu_4,
\end{aligned} \tag{31}$$

$$\begin{aligned}
\xi_k &= -\frac{l_2(\mu_k) m_3(\mu_k)}{\rho_2(\mu_k) l_2(\mu_k)}, \quad (k = 1, 2) \\
\xi_k &= -\frac{l_2(\mu_k) m_3(\mu_k)}{l_2(\mu_k) l_4(\mu_k)}. \quad (k = 4)
\end{aligned} \tag{32}$$

## 5. Formulation of exponent eigenvalue problem

In the previous sections, fundamental matrices were defined as functions of the stress and electric displacement singularity order  $\delta$ , which is an eigenvalue of a characteristic equation for a notch geometry and notch tip prescribed boundary conditions. Considering a bi-material notch as depicted in Fig. 1, where each wedge occupies the region  $0 < \theta < \omega_1$  or  $\omega_2 < \theta < 0$ , traction and charge

free notch faces impose the following boundary conditions:

$$\begin{aligned}\mathbf{T}^I(\omega_1) &= 0, \\ \mathbf{T}^{II}(\omega_2) &= 0.\end{aligned}\tag{33}$$

The bi-material interface is assumed to be coincident with  $x_1$  axis, i.e. with a nomenclature of notch faces, its wedge is  $\omega_0 = 0$ . The displacement and traction continuity is prescribed along the interface  $\omega_0 = 0$  as

$$\begin{aligned}\mathbf{u}^I(0) &= \mathbf{u}^{II}(0), \\ \mathbf{T}^I(0) &= \mathbf{T}^{II}(0).\end{aligned}\tag{34}$$

Let us consider a bi-material notch composed of two monoclinic materials, with longitudinal directions arbitrary oriented in the plane  $x_3 = 0$ . By substituting vector functions  $\boldsymbol{\lambda}(\theta)$  and  $\boldsymbol{\eta}(\theta)$  from (24) into (33) and (34), we get for the variable  $\delta$  eight homogeneous algebraic equations, which we can write in the matrix form as

$$\begin{bmatrix} \mathbf{X}_1^I & \bar{\mathbf{X}}_1^I & \mathbf{0} & \mathbf{0} \\ \mathbf{0} & \mathbf{0} & \mathbf{X}_2^{II} & \bar{\mathbf{X}}_2^{II} \\ \mathbf{B}_0^I & -\bar{\mathbf{B}}_0^I & -\mathbf{B}_0^{II} & \bar{\mathbf{B}}_0^{II} \\ \mathbf{I} & \mathbf{I} & -\mathbf{I} & -\mathbf{I} \end{bmatrix} \begin{Bmatrix} \mathbf{L}^I \mathbf{v}^I \\ \bar{\mathbf{L}}^I \mathbf{w}^I \\ \mathbf{L}^{II} \mathbf{v}^{II} \\ \bar{\mathbf{L}}^{II} \mathbf{w}^{II} \end{Bmatrix} = \mathbf{0}.\tag{35}$$

$$\mathbf{X}_j = \mathbf{L} \mathbf{Z}_j^\delta(\omega_j) (\mathbf{L})^{-1}, \quad \bar{\mathbf{X}}_j = \bar{\mathbf{L}} \mathbf{Z}_j^\delta(\omega_j) (\bar{\mathbf{L}})^{-1}, \quad (j = 1, 2)\tag{36a}$$

$$\mathbf{B}_0 = \mathbf{i} \mathbf{A} \mathbf{L}^{-1}, \quad \bar{\mathbf{B}}_0 = -\mathbf{i} \bar{\mathbf{A}} \bar{\mathbf{L}}^{-1},\tag{36b}$$

$$\mathbf{Y}_j = \bar{\mathbf{X}}_j^{-1} \mathbf{X}_j, \quad (j = 1, 2)\tag{36c}$$

where  $\mathbf{0}$  denotes  $3 \times 3$  zero matrix on the left-hand side and  $12 \times 1$  zero vector on the right-hand side of the equation. The algebraic system of the twelve equations (35) can always be reduced to the algebraic system of three equations only. Let us introduce a vector

$$\mathbf{L}_a^I \mathbf{v}_a^I = \frac{1}{2} \left( \mathbf{L}^I \mathbf{v}^I + \bar{\mathbf{L}}^I \mathbf{w}^I \right),\tag{37}$$

where index  $a$  stands for an average value of both eigenvectors  $\mathbf{L}^I \mathbf{v}^I$  and  $\bar{\mathbf{L}}^I \mathbf{w}^I$  with no physical meaning. Then the homogeneous algebraic system (35) can be eliminate to

$$\mathbf{K} \left( \mathbf{I} - \mathbf{Y}_1^I \right)^{-1} 2 \mathbf{L}_a^I \mathbf{v}_a^I = \mathbf{0},\tag{38}$$

where

$$\mathbf{K} = \mathbf{B}_0^I + \bar{\mathbf{B}}_0^I \mathbf{Y}_1^I - \left( \mathbf{B}_0^{II} + \bar{\mathbf{B}}_0^{II} \mathbf{Y}_2^{II} \right) \left( \mathbf{I} - \mathbf{Y}_2^{II} \right)^{-1} \left( \mathbf{I} - \mathbf{Y}_1^I \right).\tag{39}$$

The matrix (39) can be found also in [54] and [55], but only for the case of anisotropy and when  $\delta$  is real. To get a non-trivial solution of (38), the following relation for any  $\delta$  must be held:

$$\det [\mathbf{K}(\delta)] = 0, \quad (40)$$

which leads to a nonlinear characteristic equation, which can have unlimited number of solutions  $\delta_i$ . In the literature the solution  $\delta_i$  is sometimes called as an eigenvalue. This is mathematically not exact, but it fulfils the physical meaning. We deal only with the solutions  $\delta_i$  for which the eigenvalue of the matrix  $\mathbf{K}(\delta_i)$  equals zero. Since from the physical point of view the strain energy cannot be unbounded, the values satisfying the condition  $0 < \Re\{\delta_i\} < 1$  have to be considered. The corresponding eigenvectors  $\mathbf{v}_i^I$ ,  $\mathbf{v}_i^{II}$  and  $\mathbf{w}_i^I$ ,  $\mathbf{w}_i^{II}$  are evaluated from the expressions

$$\begin{aligned} \mathbf{v}_i^I &= (\mathbf{L}^I)^{-1} (\mathbf{I} - \mathbf{Y}_1^I)^{-1} 2\mathbf{L}_a^I \mathbf{v}_a^I, \\ \mathbf{v}_i^{II} &= (\mathbf{L}^{II})^{-1} (\mathbf{I} - \mathbf{Y}_2^{II})^{-1} (\mathbf{I} - \mathbf{Y}_1^I) \mathbf{L}^I \mathbf{v}_i^I, \\ \mathbf{w}_i^I &= -(\bar{\mathbf{L}}^I)^{-1} \mathbf{Y}_1^I \mathbf{L}^I \mathbf{v}_i^I, \\ \mathbf{w}_i^{II} &= -(\bar{\mathbf{L}}^{II})^{-1} \mathbf{Y}_2^{II} \mathbf{L}^{II} \mathbf{v}_i^{II}. \end{aligned} \quad (41)$$

The exponent  $\delta_i$  as a solution of (40) and its eigenvectors  $\mathbf{v}_i^I$ ,  $\mathbf{v}_i^{II}$  and  $\mathbf{w}_i^I$ ,  $\mathbf{w}_i^{II}$  determine the so-called regular solutions. It can be proved, see [56], that exponent  $\hat{\delta}_i = -\delta_i$  also satisfies (40). This auxiliary solution is only a mathematical tool allowing the evaluation of the GSIFs via the later introduced  $\Psi$ -integral. In fact it represents a stress field at the notch tip whose singularity is stronger than the regular one and hence with unbounded energy. By reinserting  $\hat{\delta}_i$  into (38) and by employing (41), corresponding auxiliary eigenvector  $\hat{\mathbf{v}}_i^I$  can be evaluated as well as the remaining auxiliary eigenvectors  $\hat{\mathbf{v}}_i^{II}$ ,  $\hat{\mathbf{w}}_i^I$  and  $\hat{\mathbf{w}}_i^{II}$ .

It is worth to note that the disproportion of the elastic, piezoelectric and permittivity constants causes that the matrices appearing in the constitutive laws (9) are ill-conditioned and hence the usual numerical procedures providing the evaluation of the eigennumber and eigenvectors of the matrix  $\mathbf{K}(\delta_i)$  gives wrong results. For this reason, it is suitable to use an alternative method of the evaluation of the eigenvectors  $\mathbf{v}_i^I$ ,  $\mathbf{v}_i^{II}$ ,  $\mathbf{w}_i^I$ ,  $\mathbf{w}_i^{II}$  and their auxiliary complements  $\hat{\mathbf{v}}_i^I$ ,  $\hat{\mathbf{v}}_i^{II}$ ,  $\hat{\mathbf{w}}_i^I$ ,  $\hat{\mathbf{w}}_i^{II}$ . By substituting  $\delta_i$  or  $\hat{\delta}_i$  into (38) we get

$$\mathbf{K}^*(\delta_i) \mathbf{v}_i^* = \mathbf{0}, \quad (i = 1, 2, 3) \quad (42)$$

where

$$\mathbf{K}^* = \mathbf{K} (\mathbf{I} - \mathbf{Y}_1^I)^{-1}, \quad \text{and} \quad \mathbf{v}_i^* = 2\mathbf{L}_a^I \mathbf{v}_a^I. \quad (43)$$

Equation (42) can be expressed in a matrix form as

$$\begin{bmatrix} K_{11}^{i*} & K_{12}^{i*} & K_{13}^{i*} \\ K_{21}^{i*} & K_{22}^{i*} & K_{23}^{i*} \\ K_{31}^{i*} & K_{32}^{i*} & K_{33}^{i*} \end{bmatrix} \begin{Bmatrix} v_1^{i*} \\ v_2^{i*} \\ v_3^{i*} \end{Bmatrix} = \begin{Bmatrix} 0 \\ 0 \\ 0 \end{Bmatrix}. \quad (44)$$

Because of the singularity of the matrix  $\mathbf{K}^*(\delta_i)$  the one vector component, i.e.  $v_3^{i*} = 1$ , is chosen to eliminate one row of  $\mathbf{K}^*(\delta_i)$ . System (44) is then reordered as

$$\begin{bmatrix} K_{11}^{i*} & K_{12}^{i*} \\ K_{21}^{i*} & K_{22}^{i*} \end{bmatrix} \begin{Bmatrix} v_1^{i*} \\ v_2^{i*} \end{Bmatrix} = \begin{Bmatrix} -K_{13}^{i*} \\ -K_{23}^{i*} \end{Bmatrix}. \quad (45)$$

The remaining vector components can be now solved as an ordinary system of two linear equations. In connection with the LES formalism we can define

$$2\mathbf{L}_a^I \mathbf{v}_a^I = \begin{Bmatrix} v_1^{i*} \\ v_2^{i*} \\ 1 \end{Bmatrix}. \quad (46)$$

Finally it is convenient to evaluate the eigenvector  $\mathbf{v}_i^I$  from the normalized vector  $\mathbf{L}^I \mathbf{v}_i^I$  according to the standard numerical algorithms

$$\mathbf{L}^I \mathbf{v}_i^I = \frac{\left(\mathbf{I} - \mathbf{Y}_1^I\right)^{-1} 2\mathbf{L}_a^I \mathbf{v}_a^I}{\left\| \left(\mathbf{I} - \mathbf{Y}_1^I\right)^{-1} 2\mathbf{L}_a^I \mathbf{v}_a^I \right\|}. \quad (47)$$

The remaining eigenvectors  $\mathbf{v}_i^{\Pi}$ ,  $\mathbf{w}_i^I$  and  $\mathbf{w}_i^{\Pi}$  are evaluated using (41)<sub>2</sub>–(41)<sub>4</sub>.

## 6. Determination of generalized stress intensity factors by using two-state $\Psi$ -integral

GSIFs determine the stress amplitude of the displacements, the electric potential, stresses and electrical displacements characterized by normalized shape functions (24). In the present work, GSIFs are determined by using the  $\Psi$ -integral method, which was firstly introduced in works of Sinclair et al. [57] or Vu-Quoc and Tran [58] and deeply investigated by Hwu [14]. It is based on the Betti and Rayleigh reciprocal theorem [59]. Contrary to  $J$ -integral, the maintenance on path-interdependency for  $\Psi$ -integral is also regarded for multi-material stress concentrators. Its application is conditioned by the knowledge of the so-called auxiliary solution of the particular problem, which is possible to find just by using the theory of complex potentials. Neglecting the body forces (also assumed by Lekhnitskii formalism), the  $\Psi$ -integral for a bi-material notch characterised by angles  $\omega_1$  and  $\omega_2$  becomes

$$\Psi(\mathbf{u}, \hat{\mathbf{u}}_i) = \int_{\omega_2}^{\omega_1} \left( \mathbf{u}^T \hat{\mathbf{t}}_i - \hat{\mathbf{u}}_i^T \mathbf{t} \right) r \, d\theta. \quad (48)$$

The vectors  $\hat{\mathbf{u}}_i$  and  $\hat{\mathbf{t}}_i$  are the auxiliary solutions to the displacements, tractions, electric potential and the charge and correspond to the exponent  $\hat{\delta}_i = -\delta_i$ . The auxiliary solutions are defined as

$$\begin{aligned} \hat{\mathbf{u}}_i(r, \theta) &= r^{-\delta_i} \hat{\boldsymbol{\eta}}_i(\theta), \\ \hat{\mathbf{t}}_i(r, \theta) &= -\frac{1}{r} \frac{\partial \hat{\mathbf{T}}_i(r, \theta)}{\partial \theta} = -r^{-\delta_i-1} \hat{\boldsymbol{\lambda}}_i'(\theta), \end{aligned} \quad (i = 1, 2, 3) \quad (49)$$

where  $(.)'$  denotes the differentiation with respect to  $\theta$ ,

$$\begin{aligned}\hat{\boldsymbol{\eta}}_i(\theta) &= \mathbf{A}\mathbf{Z}^{-\delta_i}(\theta)\hat{\mathbf{v}}_i + \overline{\mathbf{A}\mathbf{Z}}^{-\delta_i}(\theta)\hat{\mathbf{w}}_i, \\ \hat{\boldsymbol{\lambda}}'_i(\theta) &= \mathbf{L}\left(\mathbf{Z}^{-\delta_i}(\theta)\right)'\hat{\mathbf{v}}_i + \overline{\mathbf{L}}\left(\overline{\mathbf{Z}}^{-\delta_i}(\theta)\right)'\hat{\mathbf{w}}_i\end{aligned}\quad (i = 1, 2, 3) \quad (50)$$

and

$$\begin{aligned}\left(\mathbf{Z}^\delta(\theta)\right)' &= \text{diag}\left[\delta R_1^{\delta-1}(\theta)e^{i(\delta-1)\Psi_1(\theta)}[-\sin\theta + \mu_1\cos\theta],\right. \\ &\quad \delta R_2^{\delta-1}(\theta)e^{i(\delta-1)\Psi_2(\theta)}[-\sin\theta + \mu_2\cos\theta], \\ &\quad \left.\delta R_3^{\delta-1}(\theta)e^{i(\delta-1)\Psi_3(\theta)}[-\sin\theta + \mu_3\cos\theta]\right],\end{aligned}\quad (51)$$

$$\begin{aligned}\left(\overline{\mathbf{Z}}^\delta(\theta)\right)' &= \text{diag}\left[\delta R_1^{\delta-1}(\theta)e^{-i(\delta-1)\Psi_1(\theta)}[-\sin\theta + \bar{\mu}_1\cos\theta],\right. \\ &\quad \delta R_2^{\delta-1}(\theta)e^{-i(\delta-1)\Psi_2(\theta)}[-\sin\theta + \bar{\mu}_2\cos\theta] \\ &\quad \left.\delta R_3^{\delta-1}(\theta)e^{-i(\delta-1)\Psi_3(\theta)}[-\sin\theta + \bar{\mu}_3\cos\theta]\right].\end{aligned}\quad (52)$$

Vectors  $\mathbf{u}$  and  $\mathbf{t}$  represent displacements, electrical potential, tractions and charge of the solution, which contains the shape functions (24) of the regular expression in the analytical as well as numerical form. In the first case, the vector  $\mathbf{u}$  is given by  $(23)_1$  and the vector  $\mathbf{t}$  is given by the derivative of  $(23)_2$  with respect to  $\theta$ ,

$$\mathbf{t}(r, \theta) = -\frac{1}{r} \frac{\partial \mathbf{T}(r, \theta)}{\partial \theta} = -H_1 r^{\delta_1-1} \boldsymbol{\lambda}'_1(\theta) - H_2 r^{\delta_2-1} \boldsymbol{\lambda}'_2(\theta) - H_3 r^{\delta_3-1} \boldsymbol{\lambda}'_3(\theta). \quad (53)$$

where taking into account  $\delta = \delta_i$  in (51) and (52) one can write

$$\boldsymbol{\lambda}'_i(\theta) = \mathbf{L}\left(\mathbf{Z}^{\delta_i}(\theta)\right)'\mathbf{v}_i + \overline{\mathbf{L}}\left(\overline{\mathbf{Z}}^{\delta_i}(\theta)\right)'\mathbf{w}_i, \quad (i = 1, 2, 3) \quad (54)$$

Since the regular and corresponding auxiliary solutions are orthogonal with respect to the integral (48), i.e.

$$\Psi(r^{\delta_j}\boldsymbol{\eta}_j(\theta), r^{-\delta_i}\hat{\boldsymbol{\eta}}_i(\theta)) = \begin{cases} \text{const} \neq 0 & \text{for } i = j, \\ 0 & \text{for } i \neq j, \end{cases} \quad (55)$$

the  $\Psi$ -integral gives an important result in the GSIFs evaluation

$$\begin{aligned}\Psi(\mathbf{u}, r^{-\delta_i}\hat{\boldsymbol{\eta}}_i(\theta)) &= \Psi(r^{\delta_i}\boldsymbol{\eta}_i(\theta), r^{-\delta_i}\hat{\boldsymbol{\eta}}_i(\theta)) = \\ &= H_i \int_{\omega_2}^{\omega_1} \left( \boldsymbol{\eta}_i^\top(\theta) \hat{\boldsymbol{\lambda}}'_i(\theta) - \hat{\boldsymbol{\eta}}_i^\top(\theta) \boldsymbol{\lambda}'_i(\theta) \right) d\theta.\end{aligned}\quad (56)$$

One can see that the integral (56) is independent on the radial coordinate  $r$  and generally path-independent. It is worth to note that integration path is

counter-clockwise oriented contrary to the clockwise oriented boundary in LES formalism giving the negative sign in (53) and (49). Reorienting the boundary leads to changing the signs on  $\mathbf{t}$  and  $\hat{\mathbf{t}}$ .

The GSIFs can be covered by defining a second integral, where the vectors  $\mathbf{u}$  and  $\mathbf{t}$  in (48) of the actual state can be obtained from any other method while the virtual state are the above defined auxiliary solutions  $\hat{\mathbf{u}}$  and  $\hat{\mathbf{t}}$ . Due to the  $\Psi$ -integral path-independence, the integration contour is chosen far away from the notch tip. In the present work, the finite element method (FEM) implemented in ANSYS software [60] or FEniCS 2018.1 [61] are used to describe the real state. Let us introduce the integral

$$\begin{aligned} \Psi(\mathbf{u}^{FEM}, r_c^{-\delta_i} \hat{\boldsymbol{\eta}}_i(\theta)) &= \\ &= \int_{\omega_2}^{\omega_1} \left( (\mathbf{u}^{FEM})^\top r_c^{-\delta-1} \hat{\boldsymbol{\lambda}}'(\theta) + r_c^{-\delta} \hat{\boldsymbol{\eta}}^\top(\theta) \mathbf{t}^{FEM} \right) r_c d\theta, \end{aligned} \quad (57)$$

where  $r_c$  is the radius of the circular path remote from the notch singularity. Note that the signs follow from the orientation of the outward normal and the integration contour. The elements of the vector  $\mathbf{u}^{FEM} = [u_1^{FEM}, u_2^{FEM}, \phi^{FEM}]^\top$  are the solution of weak form (21) and hence direct output from the finite element analysis, but elements of the vector  $\mathbf{t}^{FEM}$  along the integrating contour have to be computed from the stresses using the Cauchy's formula  $t_i = \sigma_{ij} n_j$ , in a matrix form written as

$$\mathbf{t}^{FEM} = \boldsymbol{\sigma}^{FEM} \mathbf{n}, \quad (58)$$

where  $\boldsymbol{\sigma}^{FEM}$  is the two-dimensional stress tensor and  $\mathbf{n}$  is the outer normal to the domain enclosed by the circular integrating path of the radius  $r_c$  defined as

$$\boldsymbol{\sigma}^{FEM} = \begin{bmatrix} \sigma_{11}^{FEM} & \sigma_{12}^{FEM} \\ \sigma_{21}^{FEM} & \sigma_{22}^{FEM} \\ D_1^{FEM} & D_2^{FEM} \end{bmatrix}, \quad \mathbf{n} = \begin{Bmatrix} \cos(\theta) \\ \sin(\theta) \end{Bmatrix}. \quad (59)$$

It is again worth to note that there is a mismatch between the orientation of the normal vector  $\mathbf{n}$  introduced in (59) and the orientation of the normal along any curve introduced in LES formalism, see [10]. Applying the analogy with standard dot product of the vectors, the  $\Psi$ -integrals (56) and (57) project analytical and numerical solution of the same problem into the basis function of some dual function space generated by the auxiliary solutions (50). Hence both  $\Psi$ -integrals (56) and (57) are equal and the following relations are intended

$$H_i = \frac{\Psi(\mathbf{u}^{FEM}, r_c^{-\delta_i} \hat{\boldsymbol{\eta}}_i(\theta))}{\Psi(r_c^{\delta_i} \boldsymbol{\eta}_i(\theta), r_c^{-\delta_i} \hat{\boldsymbol{\eta}}_i(\theta))}. \quad (i = 1, 2, 3) \quad (60)$$

## 7. Results and discussion

Let us consider a piezoelectric bi-material notch with a local geometry and the poling directions in Fig. 1. Herein, the angles  $\alpha_1, \alpha_2$  denote the poling

material constants		PZT-4	PZT-5H	PZT-6B	PZT-7A	BaTiO <sub>3</sub>
$C_{11}^E$	$\times 10^{10}$ [Pa]	11.3	11.7	16.3	13.1	14.6
$C_{12}^E$	$\times 10^{10}$ [Pa]	7.43	5.30	6.00	7.42	6.60
$C_{23}^E$	$\times 10^{10}$ [Pa]	7.78	5.50	6.00	7.62	6.60
$C_{22}^E$	$\times 10^{10}$ [Pa]	13.9	12.6	16.8	14.8	15.0
$C_{44}^E$	$\times 10^{10}$ [Pa]	2.56	3.53	2.71	2.54	4.40
$e_{11}$	[Cm <sup>-2</sup> ]	13.8	23.3	7.10	9.50	17.5
$e_{12}$	[Cm <sup>-2</sup> ]	-6.98	-6.50	-0.90	-2.10	-4.35
$e_{26}$	[Cm <sup>-2</sup> ]	13.4	17.0	4.60	9.70	11.4
$\omega_{11}^\varepsilon$	$\times 10^{-9}$ [C(Vm) <sup>-1</sup> ]	5.47	13.0	3.40	7.35	11.2
$\omega_{22}^\varepsilon$	$\times 10^{-9}$ [C(Vm) <sup>-1</sup> ]	6.00	15.1	3.60	8.11	9.87

Table 1: The material properties of the transversally isotropic piezoelectric ceramics poled in  $x_1$ -axis [36], [17], [16].

directions. Note that the poling has a directional character, which corresponds to the polarization. It means, contrary to the fibre orientation by the anisotropic elasticity, that if we rotate the poling direction about for example  $90^\circ$  and  $-90^\circ$ , we do not obtain the same material behaviour. The only difference is in the structure of piezoelectric matrix  $\mathbf{e}$  or  $\mathbf{g}$  in (1) or (3), respectively, whose elements have opposite signs for the above mentioned rotations. We apply the extended LES formalism on common transversally isotropic piezoelectric materials, whose the elastic, piezoelectric and electric material characteristics are stated in Tab. 1. In the most papers, the material properties are defined for the poling in  $x_3$ -axis. To keep the extended LES formalism consistent with the LES formalism for the pure anisotropic elasticity, the poling direction is considered parallel with  $x_1$ -axis. The elastic, piezoelectric constants and the permittivities can be reordered by the following procedure:

$$\begin{aligned}
C_{11}^{E,x_1} &= C_{33}^{E,x_3}, C_{12}^{E,x_1} = C_{13}^{E,x_3}, \\
C_{23}^{E,x_1} &= C_{12}^{E,x_3}, C_{22}^{E,x_1} = C_{11}^{E,x_3}, \\
C_{44}^{E,x_1} &= C_{44}^{E,x_3}, \\
e_{11}^{x_1} &= e_{33}^{x_3}, e_{12}^{x_1} = e_{13}^{x_3}, e_{26}^{x_1} = e_{15}^{x_3}, \\
\omega_{11}^{\varepsilon,x_1} &= \omega_{33}^{\varepsilon,x_3}, \omega_{22}^{\varepsilon,x_1} = \omega_{11}^{\varepsilon,x_3}.
\end{aligned} \tag{61}$$

150 In many studies, the poling direction is considered parallel with any of the coordinate axes. Then, the material eigenvalues have a form  $\mu_{1,3} = \mp a + bi$ ,  $\mu_2 = ci$ . When the arbitrary fibre orientation is considered, real and imaginary parts of  $\mu_1$  and  $\mu_3$  are distinct. This is illustrated in Tab. 2 for PZT-4. Values for the poling direction  $\alpha = 90^\circ$  agree with those in [25].

155 It is worth to note that for the cases  $\alpha = 0^\circ$  and  $\alpha = 180^\circ$  we get equal eigenvalues, but as it was mentioned in the section 2, the material behaviour is



poling direction	$\mu_1$	$\mu_2$	$\mu_3$
$\alpha = 0^\circ$	$-0.2183 + 0.86483i$	$0.8396i$	$0.2183 + 0.86483i$
$\alpha = 50^\circ$	$0.0944 + 1.3004i$	$0.1266 + 0.7898i$	$0.1757 + 1.0154i$
$\alpha = 90^\circ$	$-0.2744 + 1.0871i$	$1.1910i$	$0.2744 + 1.0871i$
$\alpha = 180^\circ$	$-0.2183 + 0.86483i$	$0.8396i$	$0.2183 + 0.86483i$

Table 2: The material eigenvalues for the certain poling directions  $\alpha$  of PZT-4.

bi-materials	$\delta_1$	$\delta_2$	oscillatory index $\varepsilon$	comparison with Ou and Wu [36]
PZT-5H/BaTiO <sub>3</sub>	$0.5+0.01293i$	$0.5-0.01293i$	0.01293	0.0130
PZT-5H/PZT-6B	$0.5+0.02189i$	$0.5-0.02189i$	0.02189	0.0219
PZT-5H/PZT-7A	$0.5+0.00697i$	$0.5-0.00697i$	0.00697	0.0069
PZT-6B/PZT-7A	$0.5+0.00547i$	$0.5-0.00547i$	0.00547	0.0055

Table 3: Oscillatory indices of  $\varepsilon$ -class bi-materials and their comparison with results in [36].

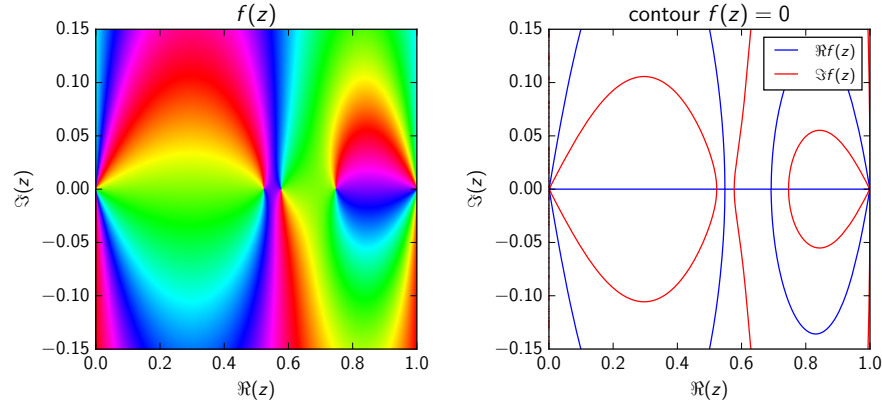


Figure 2: The HSV and contour plot of the characteristic function  $f(\delta) = \det[\mathbf{K}(\mathbf{I} - \mathbf{Y}_1^I)^{-1}]$  defined in (40) for a PZT-5H/BaTiO<sub>3</sub> bi-material notch with geometry  $\omega_1 = 120^\circ$ ,  $\omega_2 = -180^\circ$ . The intersections of the curves with different colour give the searched roots.

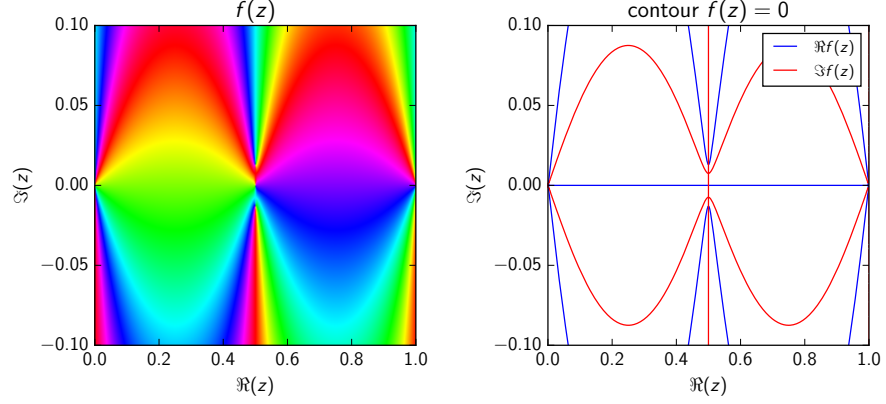


Figure 3: The HSV and contour plot of the characteristic function  $f(\delta) = \det[\mathbf{K}(\mathbf{I} - \mathbf{Y}_1^I)^{-1}]$  defined in (40) for a PZT-5H/BaTiO<sub>3</sub> bi-material notch with geometry  $\omega_1 = 180^\circ$ ,  $\omega_2 = -180^\circ$ . The intersections of the curves with different colour give the searched roots.

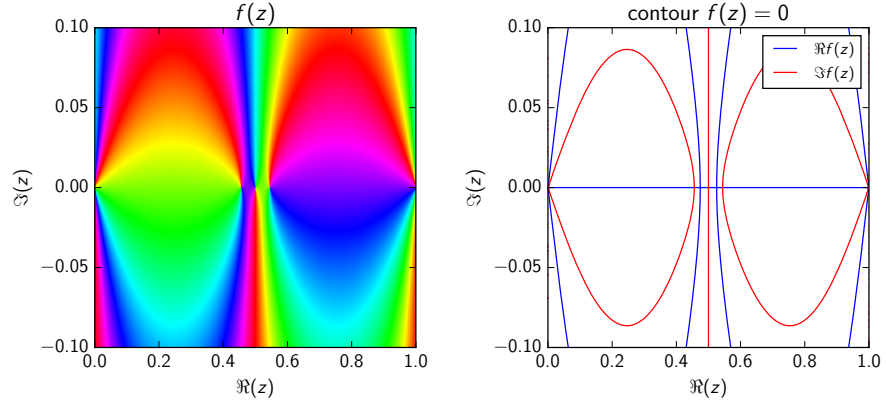


Figure 4: The HSV and contour plot of the characteristic function  $f(\delta) = \det[\mathbf{K}(\mathbf{I} - \mathbf{Y}_1^I)^{-1}]$  defined in (40) for a PZT-5H/PZT-4 bi-material notch with geometry  $\omega_1 = 180^\circ$ ,  $\omega_2 = -180^\circ$ . The intersections of the curves with different colour give the searched roots.

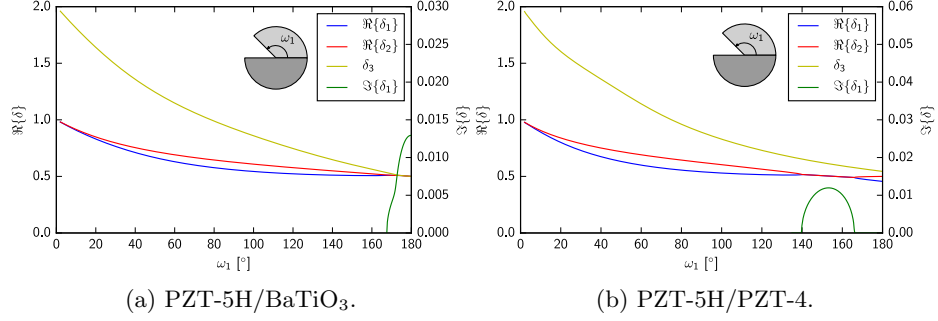


Figure 5: The exponent  $\delta_i$  dependence on the notch geometry  $\omega_1$ . Poling directions are  $\alpha_1 = 90^\circ$ ,  $\alpha_2 = 90^\circ$ .

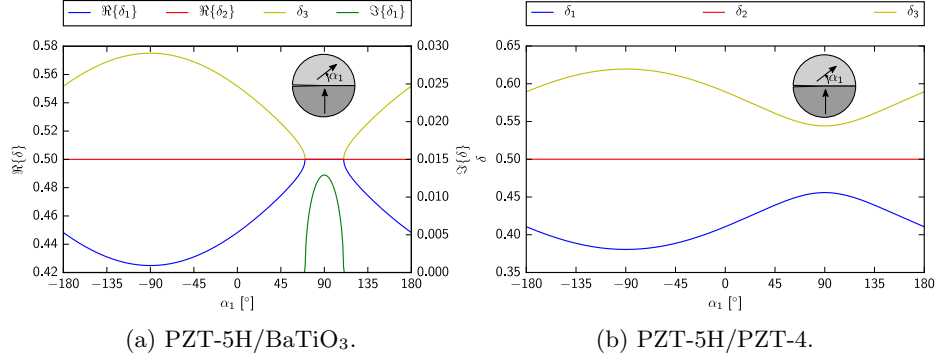


Figure 6: The dependence of the interface crack exponents  $\delta_i$  on the poling direction  $\alpha_1$ . The poling direction  $\alpha_2 = 90^\circ$ .

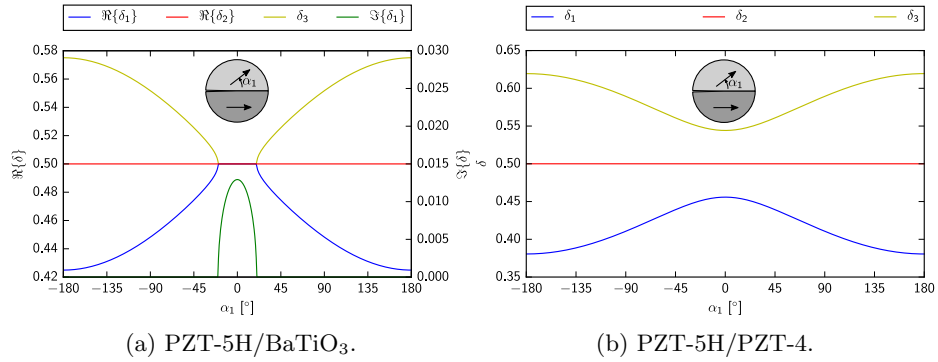


Figure 7: The dependence of the interface crack exponents  $\delta_i$  on the poling direction  $\alpha_1$ . The poling direction  $\alpha_2 = 0^\circ$ .

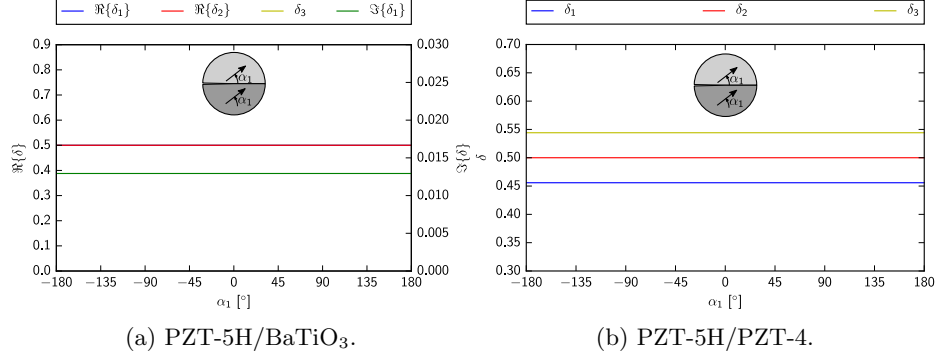


Figure 8: The dependence of the interface crack exponents  $\delta_i$  on the poling direction  $\alpha_1$ . The poling direction  $\alpha_2 = \alpha_1$ .

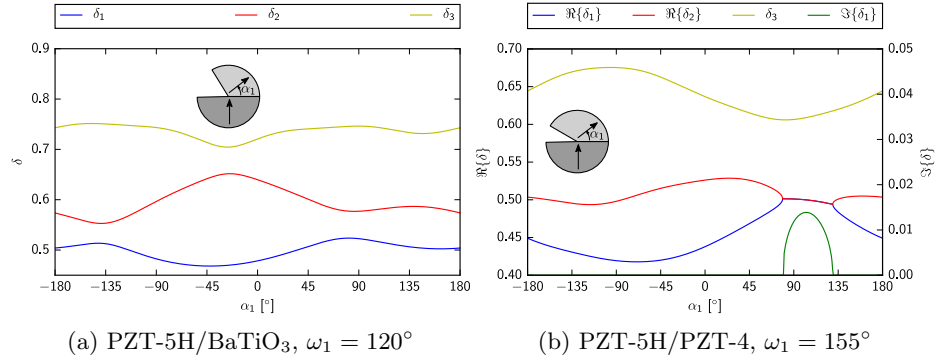


Figure 9: Dependence study of the singular stress terms  $\delta$  on the poling direction  $\alpha_1$  of two cases of a bi-material notch. Poling direction  $\alpha_2 = 90^\circ$ .

bi-materials	$\delta_1$	$\delta_3$	oscillatory index $\kappa$	comparison with Ou and Wu [36]
PZT-4/BaTiO <sub>3</sub>	0.44914	0.55086	0.05086	0.0508
PZT-4/PZT-5H	0.45585	0.54415	0.04415	0.0442
PZT-4/PZT-6B	0.48316	0.51684	0.01684	0.0168
PZT-4/PZT-7A	0.47525	0.52475	0.02475	0.0247
PZT-6B/BaTiO <sub>3</sub>	0.49039	0.50961	0.00961	0.0095
PZT-7A/BaTiO <sub>3</sub>	0.47936	0.52064	0.02064	0.0206

Table 4: Oscillatory indices of  $\kappa$ -class bi-materials and their comparison with results in [36].

different due to the opposite signs in the piezoelectric matrix  $\hat{\mathbf{g}}'$ .

Let us consider the PZT-5H/BaTiO<sub>3</sub> of material 1/material 2 combination and a bi-material notch given by  $\omega_1 = 120^\circ$  and  $\omega_2 = -180^\circ$ . In all of the following examples, poling direction is parallel with  $x_2$ -axis ( $\alpha_1 = \alpha_2 = 90^\circ$ ) if it is not specified otherwise. The phase portrait of the transcendental function (40) is depicted in Fig. 2. There are three real roots  $\delta_1 = 0.5226$ ,  $\delta_2 = 0.5770$  and  $\delta_3 = 0.7462$  of the characteristic function (40) in the interval  $0 < \Re\{\delta\} < 1$ . In a case of an interface crack ( $\omega_1 = 180^\circ$ ), there are two complex conjugate roots  $\delta_1 = 0.5 + 0.01293i$ ,  $\delta_2 = 0.5 - 0.01293i$  and the third one  $\delta_3 = 0.5$ , see Fig. 3. The characteristic function (40) has two poles at the points  $\delta = 0$  and  $\delta = 1$  in both notch configurations.

The different results are obtained when we consider an interface crack between PZT-5H and PZT-4 materials. One can see that there are three real roots:  $\delta_1 = 0.4558$ ,  $\delta_2 = 0.5$  and  $\delta_3 = 0.5442$  in the graphs on Fig. 4 contrary to complex ones in the previous material combination. The disappearing of the oscillatory index  $\varepsilon$  is can be given by comparing the results with Ou and Wu [36]. Here, the interface crack was investigated as the Hilbert problem, e.g. [33], and it was found out that there are two types of singularities in the case of interface crack between two piezoelectric material - the oscillatory singularity when exponents have an oscillatory index  $\varepsilon$ , and the non-oscillatory singularity when exponents have oscillatory index  $i\kappa$ . In the first case, the eigenvalues have the form

$$\delta_{1,2} = 0.5 \pm i\varepsilon, \quad (62)$$

while in the latter case

$$\delta_{1,3} = 0.5 \pm i(i\kappa) = 0.5 \mp \kappa, \quad (63)$$

which are real numbers. The bi-materials with an interface crack are then divided into two classes:  $\varepsilon$ -class and  $\kappa$ -class. Contrary to the Hilbert problem  
170 formulation showed in [36], the employed procedure solving the eigenvalue problem (35) and (36) for  $\kappa$ -class bi-materials does not get the oscillatory indices  $i\kappa$  and the value 0.5 in the found exponent  $\delta$  separately, but absorbed in the resulting roots of the equation (40). When we take a look at the exponents for the PTZ-5H/PZT-4 bi-material more closely, we see that  $\delta_1$  and  $\delta_3$  are sym-  
175 metric with respect to the  $\delta_2 = 0.5$ . Then the parameter  $\kappa$  can be extracted by subtracting the value 0.5 from  $\delta_1$  or  $\delta_2$ , respectively. The observed results of  $\delta_1$  and  $\delta_2$  for all material combinations compared with the values given in the literature are summarized in Tab. 3 and Tab. 4. The Tab. 4 gives the parameter  $\kappa$  extracted from the found exponent using the equation (63). The remaining  
180 exponent is always gets the value  $\delta_3 = 0.5$  for all bi-material combinations. One can see that the all received values of  $\delta_1$  and  $\delta_2$  coincide with the values given in [36].

A study of the dependence of the exponents  $\delta_i$  on the notch angle  $\omega_1$  shows us more about the differences between particular bi-material classes. Let the angle  
185  $\omega_2 = -180^\circ$  be fixed and the angle  $\omega_1$  change in the interval  $0 < \omega_1 < 180^\circ$ . The dependence of the exponents  $\delta_i$ , for PZT-5H/BaTiO<sub>3</sub> bi-material on the angle  $\omega_1$  is depicted in the Fig. 5a. Similar development can be obtained for all  $\varepsilon$ -class bi-materials. Eigenvalues  $\delta_1$  and  $\delta_2$  are real valued in the almost whole interval  $0 < \omega_1 < 180^\circ$  except the values for  $\omega_1 > 168^\circ$ , when they become complex  
190 conjugate. Note that imaginary part of  $\delta_2$  is not depicted because it has the same values as  $\Im\{\delta_1\}$  but with opposite sign. Third eigenvalue  $\delta_3$  corresponds to the non-singular character of the stress and electric displacement field at the notch tip because  $\delta_3 > 1$  up to  $\omega_1 = 78^\circ$  and it is always real. Real parts of complex conjugate eigenvalues  $\delta_1$  and  $\delta_2$  as well as the third one  $\delta_3$  converge to  
195 the value 0.5 for  $\omega_1 \rightarrow 180^\circ$ . It has to be pointed out that  $\delta_3$  is not equal to the real parts of neither  $\delta_1$  nor  $\delta_2$  for very closed notch configurations.

The same study was done for PZT-5H/PZT4 bi-material, a representative one of the  $\kappa$ -class. One can see in Fig. 5b the different dependency of the exponents  $\delta_i$  on the  $\omega_1$  contrary to the previous study. The third eigenvalue  $\delta_3$   
200 provides the stress and electric displacement field at the notch tip singular when  $\delta_3 < 1$  for  $\omega_1 > 75^\circ$ . Moreover it is real in the whole interval  $0 < \omega_1 < 180^\circ$ . The exponents  $\delta_1$  and  $\delta_2$  are complex conjugate for  $139^\circ < \omega_1 < 166^\circ$ . For the interface crack as the limit case of the notch, the exponent  $\delta_2$  converges to 0.5, while the exponents  $\delta_1$  and  $\delta_3$  become symmetric with respect to the exponent  
205  $\delta_2$ . The same bi-material was investigated by Hirai et al. [16]. Unfortunately their outputs and the results publish here mismatch.

Comparing the graphs in Fig. 5 one can see that by considering a bi-material notch defined by an arbitrary angle  $\omega_1$ , the bi-material classification introduced by Ou and Wu [36] for interface cracks is ambiguous for general stress concentra-  
210 tors  $H_i$ . Whereas PZT-5H/BaTiO<sub>3</sub> bi-material only has the  $\varepsilon$ -type oscillatory index, the material combination PZT-5H/PZT-4 has both oscillatory indices -  $\varepsilon$  as well as  $\kappa$ , but for certain angles  $\omega_1$  including the case of the interface crack. Actually, a bi-material solved via the eigenvalue problem (35) and (36) has only

the  $\varepsilon$  oscillatory index and as it is mentioned above, the parameter  $\kappa$  is absorbed  
 215 in the real roots observed in the case of an interface crack.

This discrepancy can be seen also by performing a study of the dependency  
 of the exponents  $\delta_i$  on an poling angle  $\alpha_1$  while the angle  $\alpha_2 = 90^\circ$  remains fixed.  
 The Figs. 6a and 6b show the exponents  $\delta_i$  of the bi-materials composed of two  
 typical piezoelectric materials. The PZT-5H/BaTiO<sub>3</sub> bi-material combination  
 220 in Fig. 6a has two complex conjugate exponents  $\delta_1$  and  $\delta_2$  in a small interval  
 $70^\circ < \alpha_1 < 90^\circ$  while their real parts are equal to 0.5. The third exponent is  
 constant  $\delta_3 = 0.5$ . The exponents  $\delta_1$  and  $\delta_3$  become abruptly real and symmetric  
 with respect to  $\delta_2$  for the remaining values of  $\alpha_1$ . The PZT-5H/PZT-4 bi-  
 material has the real exponents  $\delta_i$  only. In both bi-materials the same poling  
 225 orientation  $\alpha_1 = \alpha_2 = 90^\circ$  leads to the fact, that the real parts of the exponents  
 $\delta_i$  are equal or have the closest value to the value 0.5. It means, that the  
 stress and electric displacement singularity at the tip of the interface crack is  
 the strongest one in this case. The same parallelism effect of poling directions  
 of the both materials in the cracked bi-material show Figs. 7a and 7b, but  
 230 for the case of  $\alpha_1 = \alpha_2 = 0$ . A fact that the always parallel poling directions  
 maximizing the singularity of the stress and electric displacement field can be  
 arbitrary is illustrated in Fig. 8, where the values of the exponents  $\delta_i$  remain  
 constant for any value  $\alpha_1 = \alpha_2$ .

Let us perform the same studies for non-symmetric notches. Two charac-  
 235 teristic notch configurations has been investigated to get an idea about the  
 exponents  $\delta_i$  behaviour. Considering the PZT-5H/BaTiO<sub>3</sub> bi-material defined  
 by  $\omega_1 = 120^\circ$  and  $\omega_2 = 180^\circ$ . We see in Fig. 5 that there are three real expo-  
 nents  $\delta_i$ . The Fig. 9a shows that by changing poling direction  $\alpha_1$  the exponents  
 $\delta_i$  remain real. In contrast to that result, PZT-5H/BaTiO<sub>3</sub> bi-material has two  
 240 complex conjugate exponents  $\delta_1, \delta_2$  and the real one  $\delta_3$  for  $80^\circ < \alpha_1 < 130^\circ$ .  
 It also has three real exponents  $\delta_i$  for the remaining values  $0 < \alpha_1 < 80^\circ$  and  
 $130^\circ < \alpha_1 < 180^\circ$ . Similar development can be seen in Chen [28] for a right  
 angle bonded wedge for PZT-5H/PZT-4 bi-material. We can see that the  $\varepsilon$  and  
 $\kappa$  classification of a bi-material is applicable only for an interface crack. From  
 245 the above investigation we can claim that a bi-material notch problem solved by  
 (35) and (36) can have either three real exponents  $\delta_i$  or two complex conjugates  
 exponents  $\delta_1, \delta_2$  with an oscillatory index  $\varepsilon$  and one real exponent  $\delta_3$ . Closing  
 a notch by  $\omega_1 \rightarrow 180^\circ$ , we get two unique exponent developments - type A (Fig.  
 5a) or type B (Fig. 5b). Their limit states, an interface crack for  $\omega_1 = 180^\circ$ ,  
 250 has either three real exponents (two  $\delta_1$  and  $\delta_3$  symmetric with respect to third  
 one  $\delta_2 = 0.5$ ) or two complex conjugate exponents  $\delta_1, \delta_2$  with real parts 0.5  
 and one real exponent  $\delta_3 = 0.5$ . However, by changing the poling direction  $\alpha_1$ ,  
 bi-materials can switch from one to another set of exponents  $\delta_i$ . Furthermore,  
 the interface crack is the only one concentrator when the symmetry of two ex-  
 ponents, e.g.  $\delta_1$  and  $\delta_3$ , with respect to the third one  $\delta_3$  occurs. That is the  
 255 reason why the classification introduced in Ou and Wu [36] cannot be used in  
 the present study for general singular stress concentrators.

The knowledge of the character of the stress and electric displacement sin-  
 gularity represented by the exponents  $\delta_i$  is necessary to the GSIFs evaluation

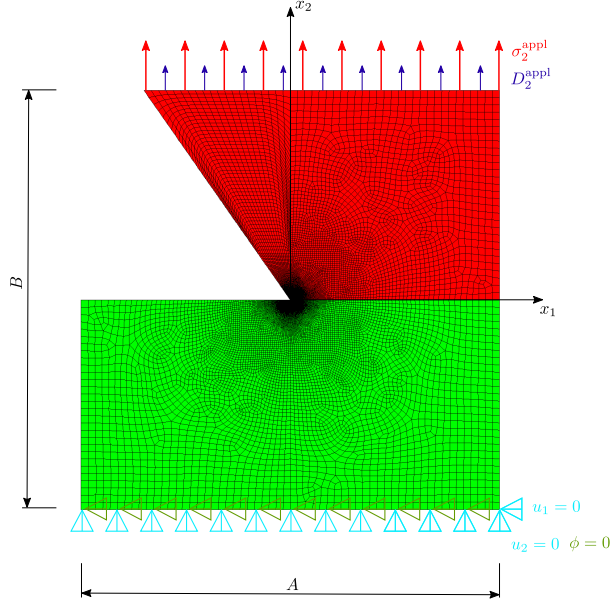
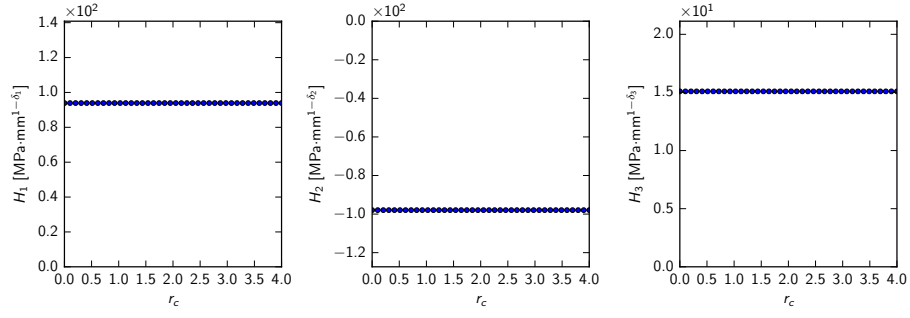


Figure 10: Finite element mesh of the piezoelectric bi-material notch model with mechanical and electrical boundary conditions.

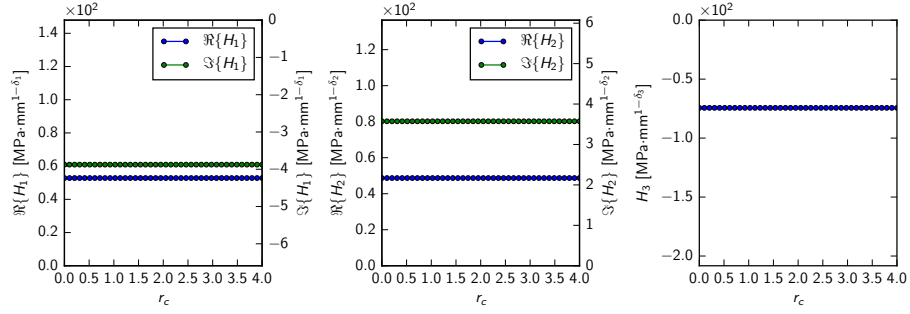
discussed in the following. The FEM analysis is another required component of the procedure allows one to get complete description of the singular stress and electric displacement field at the bi-material notch tip. The FEM results are computed by softwares ANSYS and FEniCS. Both of them give the same result. The 8-node quadratic plane element `PLANE223` for coupled field analyses was used with the option of plane strain state (generalized plane strain and short circuit:  $\varepsilon_3 = 0$  and  $E_3 = 0$ ) in the case of the using ANSYS. By setting `KEYOPT,e_type,1,1001` electrostatic-structural coupled field analysis with piezoelectric effect is enabled. Variable notch geometry is enabled, face angles  $\omega_1, \omega_2$  could attain values between  $0^\circ$  and  $180^\circ$  while bi-material interface remains fixed at  $\omega_0 = 0^\circ$ . Fibre orientation is realized by orienting the element coordinate system by angles  $\alpha_1$  and  $\alpha_2$ , respectively. Dimensions of the two-dimensional model are  $A = 180$  mm and  $B = 180$  mm. In the case of the FEniCS solver, the 6-node standard triangle Lagrange element of the discrete function space  $V_{\mathbf{u}}$  and  $V_\phi$  as the subsets of the Hilbert space  $H^1$  are chosen. The FEniCS then solves the weak formulation (21) as the mixed problem  $(\mathbf{u}, \phi) \in V_{\mathbf{u}} \times V_\phi$ , for details see the FEniCS script in Appendix A.

The notch geometry and boundary conditions are illustrated in Fig. 10. Displacements at the right lateral node are fixed in the  $x_1$  direction in order to avoid rigid body motion. The applied stress  $\sigma_{22}^{\text{appl}} = 10$  kPa and the electric displacement is  $D_2^{\text{appl}} = 0.01$  Cm $^{-2}$ . Displacement  $u_2$  on the upper boundary is coupled in order to minimize the non-uniform loading. According to the elec-





(a) PZT-5H/PZT-4,  $\omega_1 = 120^\circ$



(b) PZT-5H/BaTiO<sub>3</sub>,  $\omega_1 = 180^\circ$

Figure 11: The dependency of the GSIFs on the radius  $r_c$  of the integration path enclosing (a) the piezoelectric bi-material notch given by  $\omega_1 = 120^\circ$ ,  $\delta_1 = 0.5226$ ,  $\delta_2 = 0.5770$ ,  $\delta_3 = 0.7462$  and (b) the piezoelectric interface crack given by  $\delta_1 = 0.5 + 0.01293i$ ,  $\delta_2 = 0.5 - 0.01293i$ ,  $\delta_3 = 0.5$ .

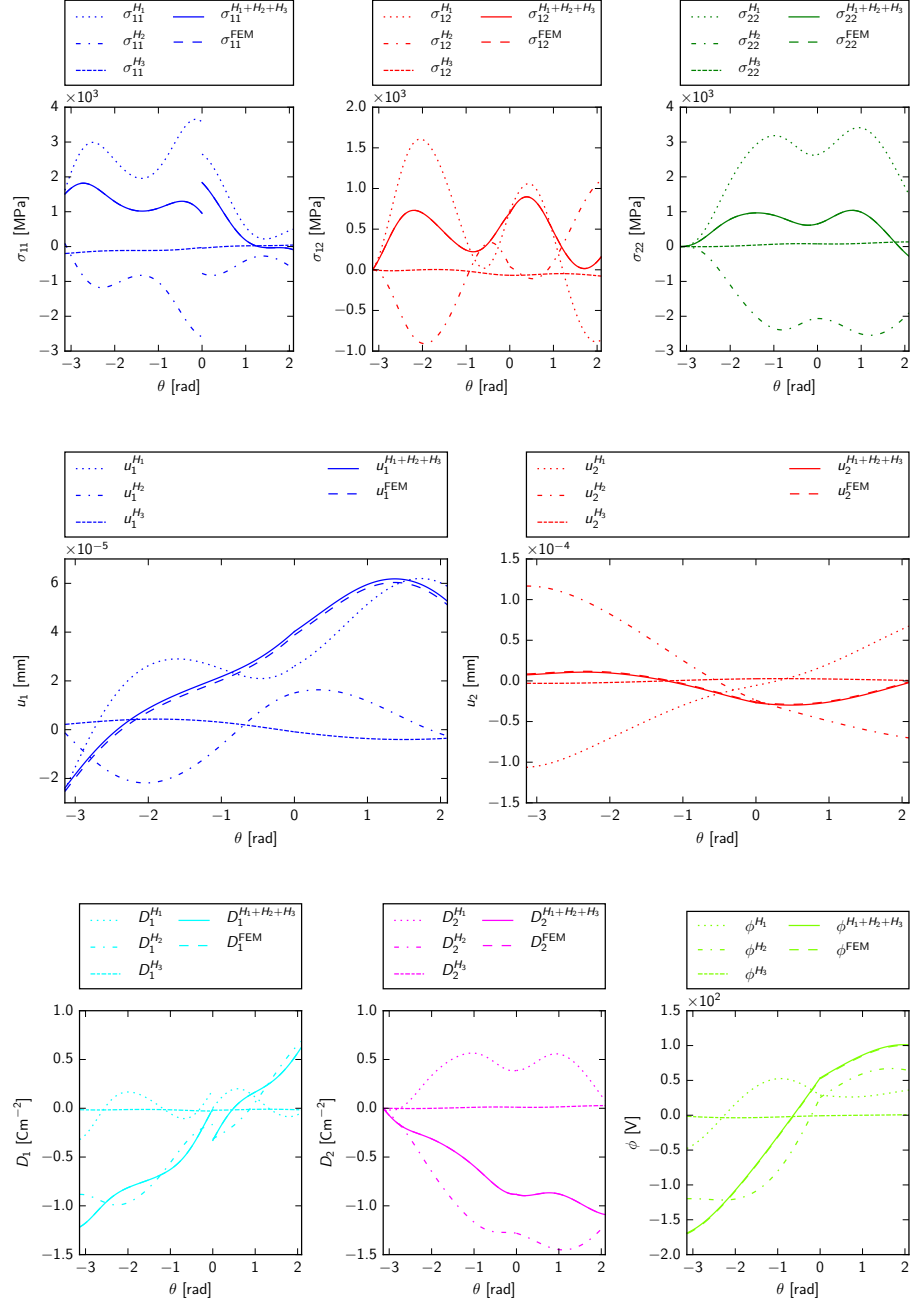


Figure 12: The displacements, stress components, electric displacement components and electric potential of PZT-5H/PZT-4 bi-material notch on the circular path  $r = 0.001$  mm,  $\omega_1 = 120^\circ$ ,  $\omega_2 = -180^\circ$ .

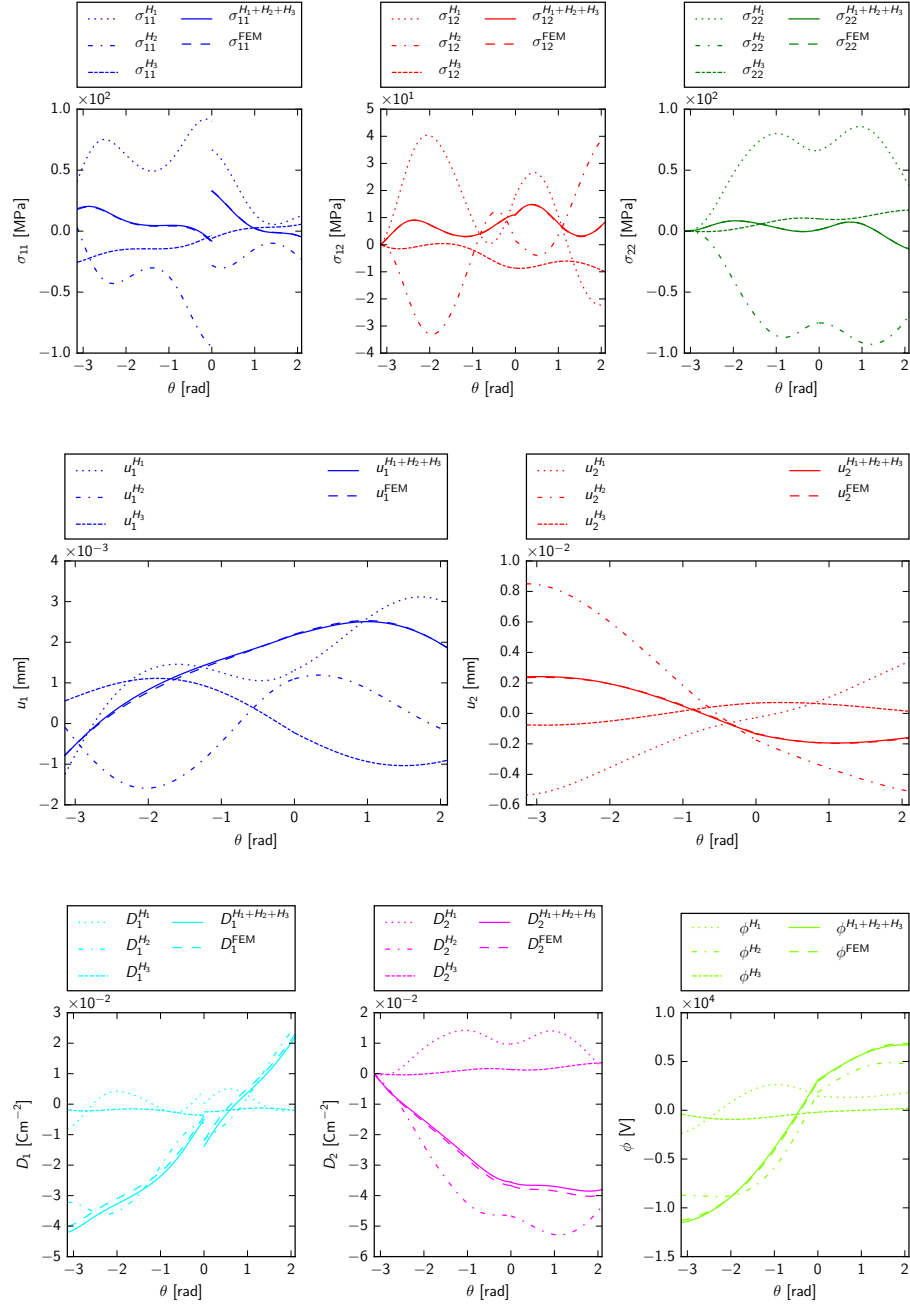


Figure 13: The displacements, stress components, electric displacement components and electric potential of PZT-5H/PZT-4 bi-material notch on the circular path  $r = 2$  mm,  $\omega_1 = 120^\circ$ ,  $\omega_2 = -180^\circ$ .

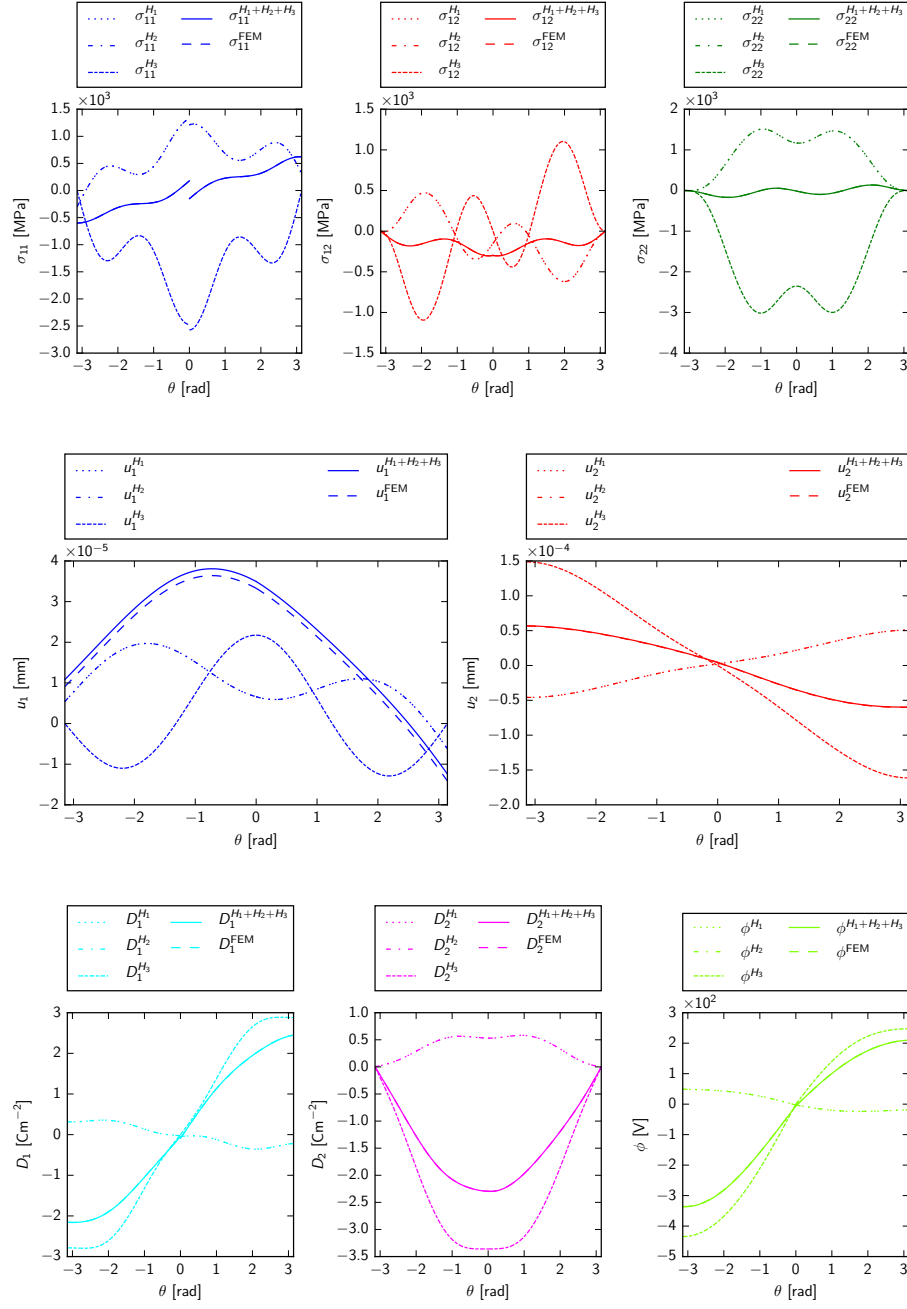


Figure 14: The displacements, stress components, electric displacement components and electric potential of PZT-5H/BaTiO<sub>3</sub> bi-material notch on the circular path  $r = 0.001$  mm,  $\omega_1 = 180^\circ$ ,  $\omega_2 = -180^\circ$ .

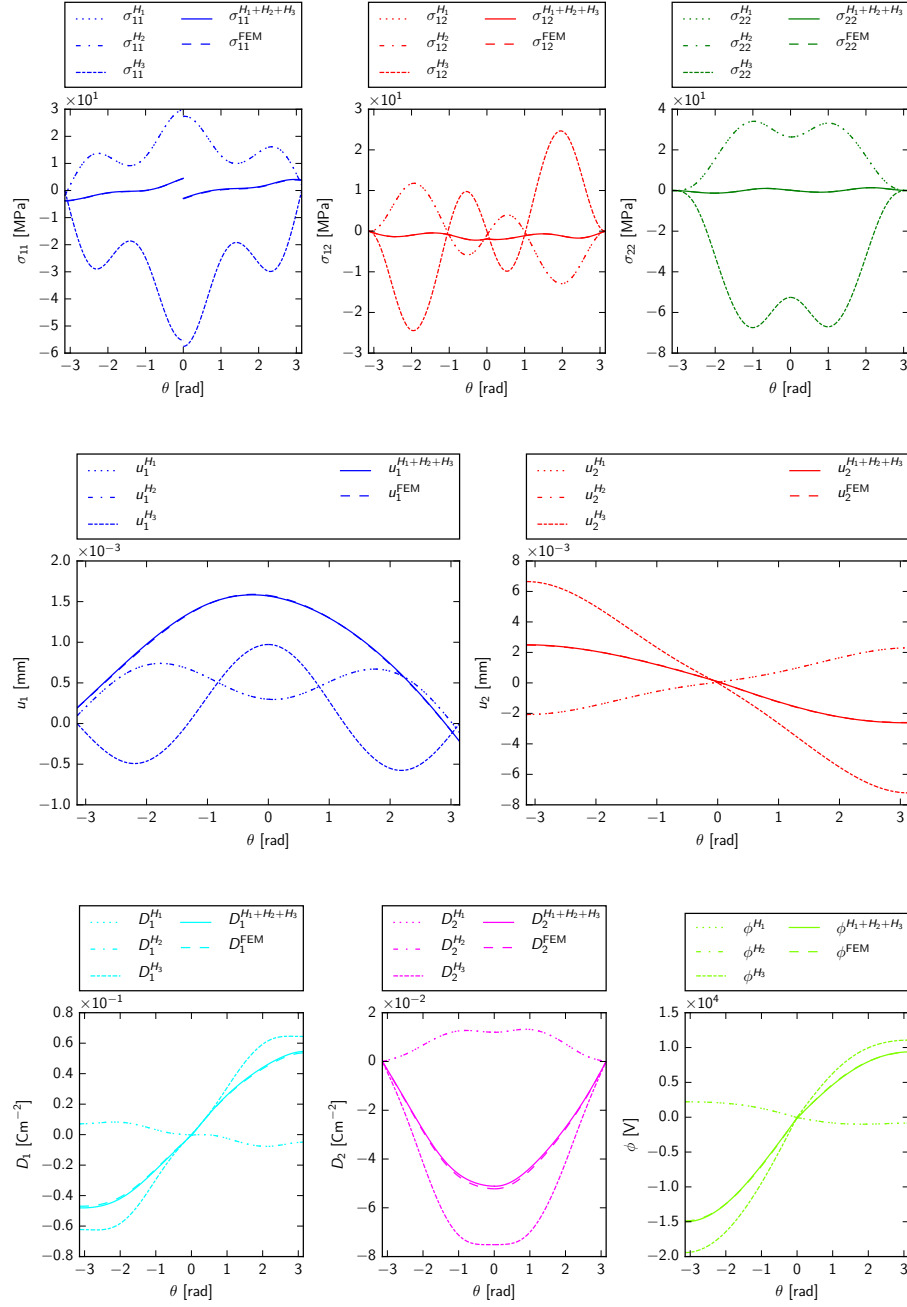


Figure 15: The displacements, stress components, electric displacement components and electric potential of PZT-5H/BaTiO<sub>3</sub> bi-material notch on the circular path  $r = 2$  mm,  $\omega_1 = 180^\circ$ ,  $\omega_2 = -180^\circ$ .

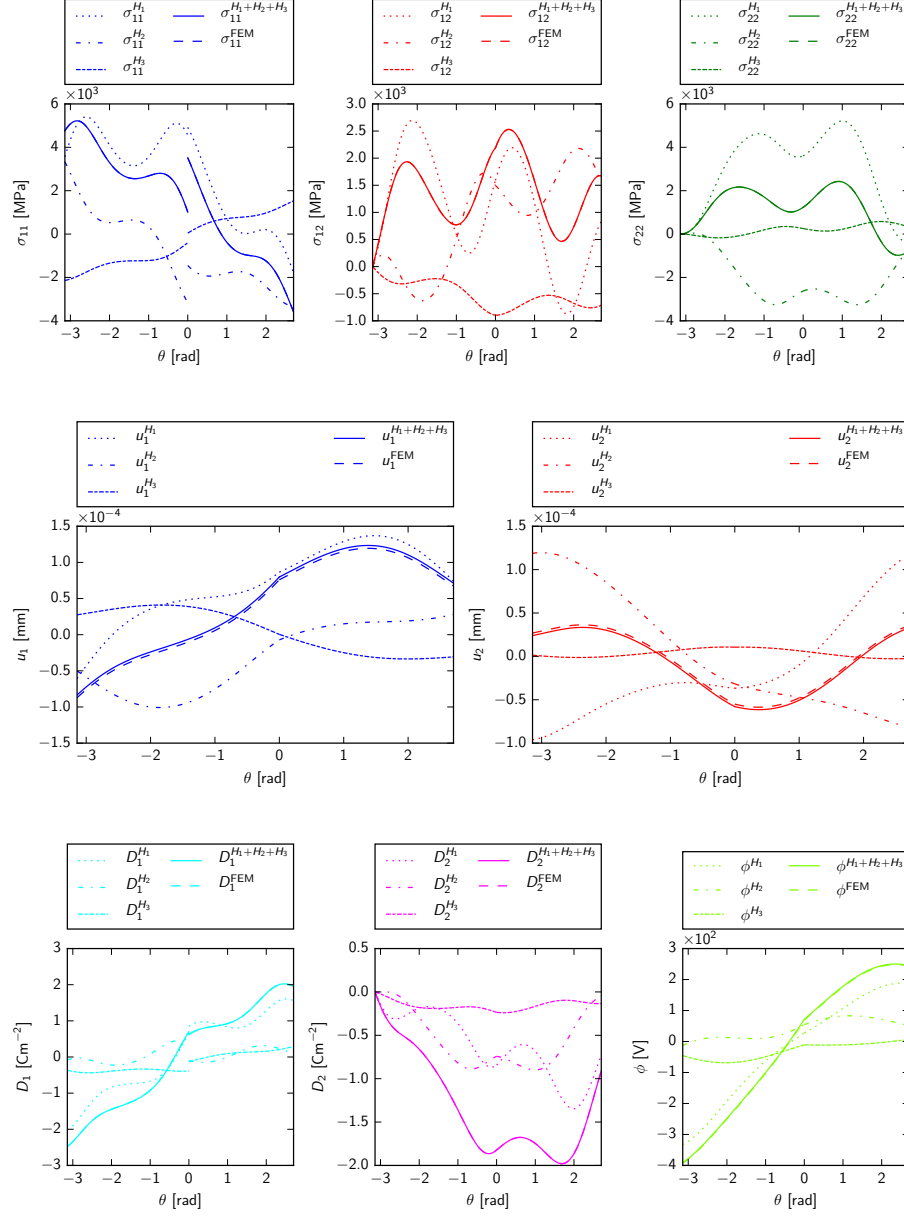


Figure 16: The displacements, stress components, electric displacement components and electric potential of PZT-5H/PZT-4 bi-material notch on the circular path  $r = 0.001$  mm,  $\omega_1 = 155^\circ$ ,  $\omega_2 = -180^\circ$ . Poling directions are  $\alpha_1 = 40^\circ$  and  $\alpha_2 = 90^\circ$ .

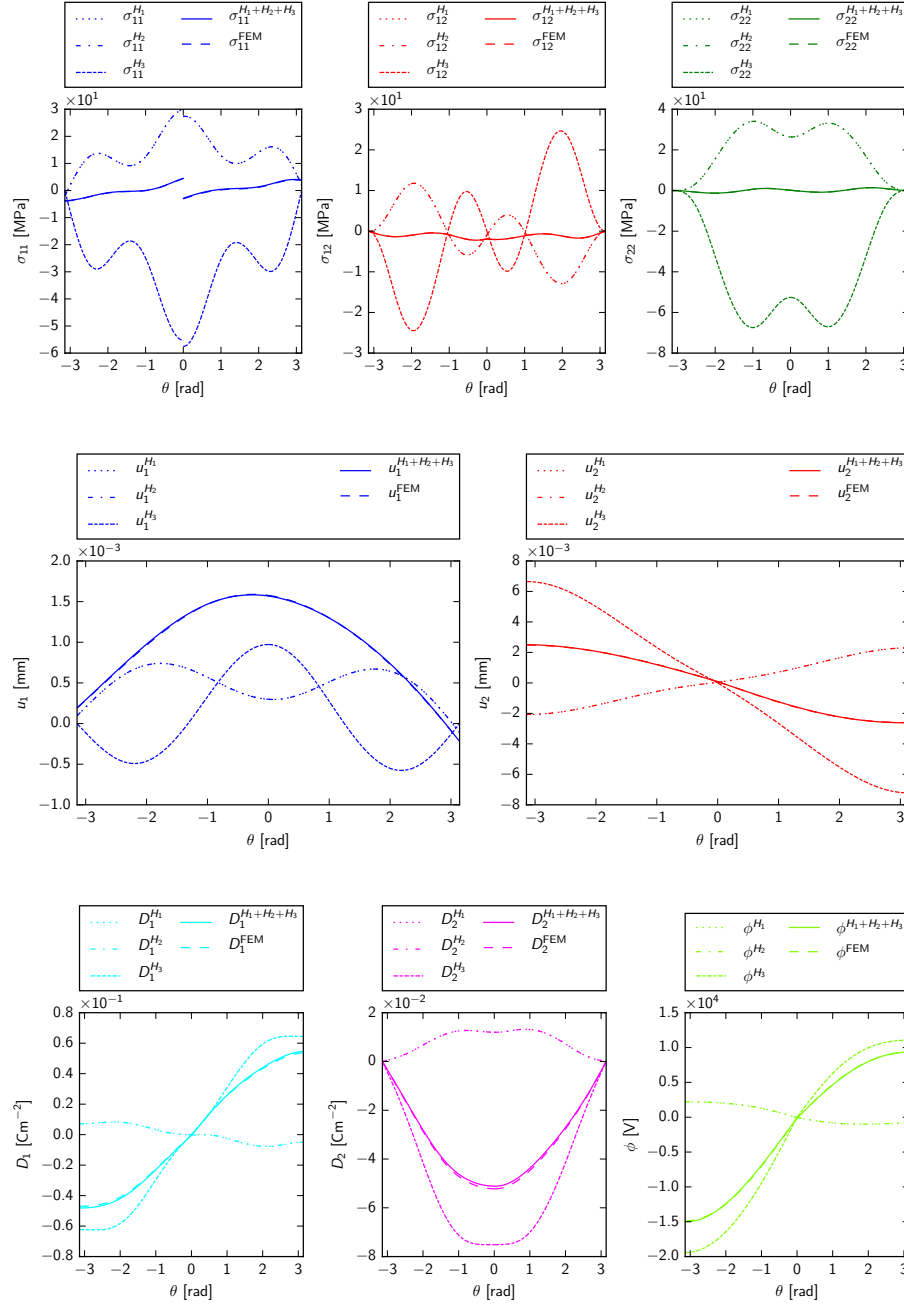


Figure 17: The displacements, stress components, electric displacement components and electric potential of PZT-5H/PZT-4 bi-material notch on the circular path  $r = 2$  mm,  $\omega_1 = 155^\circ$ ,  $\omega_2 = -180^\circ$ . Poling directions are  $\alpha_1 = 40^\circ$  and  $\alpha_2 = 90^\circ$ .

285 tromechanical analogy, electric potential  $\phi$  is also coupled. Coordinate systems of the deformed FEM solution and the analytical solution (23)<sub>1</sub> are not coincident, hence the both notch tip displacements and electric potential have to be subtracted from all body displacements and potential, respectively. It has to be reminded that notch faces have to remain mechanically and electrically unloaded (zero tractions  $\mathbf{t}$  and the charge  $q$ ).

290 The numerical integration of the  $\Psi$ -integrals in (60) is realized by the Romberg's integration method. The advantage of this method contrary to e.g. the trapezoidal rule is that it enables the usage of the adaptive integration step and achieves the better accuracy. Therefore, an interpolation function of the nodal results has to be created in order to get approximative value in an arbitrary point. For the interpolation, the linear interpolation function has to be used. From the computational point of view, integrals are evaluated for each material region separately, because if we would perform the integration for the whole path from  $\omega_2$  to  $\omega_1$ , the discontinuity of  $\sigma_{11}$  would cause a numerical error. The resulting integral for the whole curve are the sum of the particular integrals.

295 In the first, the path-dependency of the  $\Psi$ -integrals is tested. The values of the GSIFs calculated via the  $\Psi$ -integrals (60) for the radii  $0.0005 \text{ mm} < r_c < 4 \text{ mm}$  are shown in Fig. 11. The study is investigated for two representative cases: bi-material notch PZT-5H/PTZ-4 with the face angles  $\omega_1 = 120^\circ$ ,  $\omega_2 = -180^\circ$ , which has real exponents  $\delta_i$  and an interface crack for PZT-5H/BaTiO<sub>3</sub> with two complex conjugate exponents  $\delta_1$ ,  $\delta_2$  and one real  $\delta_3$ . The complex intensity factors are decomposed to real and imaginary parts. One can see 300 that the graphs confirm the above mentioned independency of the  $\Psi$ -integral on its integration path. It has to be pointed out that the default settings of the integration algorithm are inappropriate to get the results in Fig. 11. The third components of the eigenvectors  $\mathbf{v}$  and  $\mathbf{w}$  from (41) are much more lower in comparison to the other ones (about ten times). That bring about problems with 310 relative tolerance in the Romberg's integration procedure, which default value is  $1.48 \times 10^{-8}$ . But this is higher than the order of the  $\Psi$ -integrals appearing in the denominators of 60 i.e. in the  $\Psi$ -integrals combining the auxiliary and regular solutions (24)<sub>1</sub>, (50) and (54). Based on that fact and additional studies it is found out that the relative error has to be set to  $1.48 \times 10^{-25}$  to get 315 precise results for all bi-material and path radius  $r_c$  configurations. For the next studies, the value  $r_c = 2 \text{ mm}$  is chosen as the radius of the integration path of the  $\Psi$ -integrals in (60).

In the following we focus on the two just above investigated bi-material configuration, i.e. PZT-5H/PST-4 and PZT-5H/BaTiO<sub>3</sub>, respectively. Since from the exponent eigenvalue problem (35) point of view only two cases can occur - three real exponents  $\delta_i$  in the first case or two complex conjugate exponents  $\delta_1$ ,  $\delta_2$  with one real  $\delta_3$  in the second case. Let us introduce the functions

$$\begin{aligned}\tilde{\lambda}_i^{x_2}(\theta) &= \mathbf{L}\delta_i \mathbf{Z}^{\delta_i-1}(\theta) \boldsymbol{\mu} \mathbf{v}_i + \bar{\mathbf{L}}\delta_i \bar{\mathbf{Z}}^{\delta_i-1}(\theta) \bar{\boldsymbol{\mu}} \mathbf{w}_i, \\ \tilde{\lambda}_i^{x_1}(\theta) &= \mathbf{L}\delta_i \mathbf{Z}^{\delta_i-1}(\theta) \mathbf{v}_i + \bar{\mathbf{L}}\delta_i \bar{\mathbf{Z}}^{\delta_i-1}(\theta) \mathbf{w}_i,\end{aligned}\quad (i = 1, 2, 3) \quad (64)$$



where

$$\boldsymbol{\mu} = \begin{bmatrix} \mu_1 & 0 & 0 \\ 0 & \mu_2 & 0 \\ 0 & 0 & \mu_3 \end{bmatrix}, \quad \bar{\boldsymbol{\mu}} = \begin{bmatrix} \bar{\mu}_1 & 0 & 0 \\ 0 & \bar{\mu}_2 & 0 \\ 0 & 0 & \bar{\mu}_3 \end{bmatrix}. \quad (65)$$

Then for the stresses and electric displacements we can write

$$\begin{aligned} \boldsymbol{\sigma}^1(r, \theta) &= -H_1 r^{\delta_1-1} \tilde{\boldsymbol{\lambda}}_1^{x_2}(\theta) - H_2 r^{\delta_2-1} \tilde{\boldsymbol{\lambda}}_2^{x_2}(\theta) - H_3 r^{\delta_3-1} \tilde{\boldsymbol{\lambda}}_3^{x_2}(\theta), \\ \boldsymbol{\sigma}^2(r, \theta) &= H_1 r^{\delta_1-1} \tilde{\boldsymbol{\lambda}}_1^{x_1}(\theta) + H_2 r^{\delta_2-1} \tilde{\boldsymbol{\lambda}}_2^{x_1}(\theta) + H_3 r^{\delta_3-1} \tilde{\boldsymbol{\lambda}}_3^{x_1}(\theta), \end{aligned} \quad (66)$$

where

$$\boldsymbol{\sigma}^1 = \begin{Bmatrix} \sigma_{11} \\ \sigma_{12} \\ D_1 \end{Bmatrix}, \quad \boldsymbol{\sigma}^2 = \begin{Bmatrix} \sigma_{21} \\ \sigma_{22} \\ D_2 \end{Bmatrix}. \quad (67)$$

Let us consider poling directions  $\alpha_1 = 90^\circ$  and  $\alpha_2 = 90^\circ$  of the bi-material and notch geometry  $\omega_1 = 120^\circ$  and  $\omega_2 = -180^\circ$ . All characteristics, the stresses and electric displacements  $\boldsymbol{\sigma}^1$  and  $\boldsymbol{\sigma}^2$ , respectively, and displacements with electrical potential  $\mathbf{u}$  using the equations (66) and (23) for the PZT-5H/PZT-4 bi-material notch on the path with radius  $r = 0.001$  mm are depicted in Fig. 12 and shows very good correspondence with the FEM solution. Also here we can see that the values closest to  $\Re\{\delta\} = 0.5$  have the strongest contribution to the resulting final stress field. The same calculation but for the radius  $r = 2$  mm, are depicted in Fig. 13. We can see that the correspondence is still very good, more significant changes are present in electric displacements.

The stresses, electric displacements, displacements and electric potentials at the interface crack tip in the bi-material PZT-5H/BaTiO<sub>3</sub> on the paths with radii  $r = 0.001$  mm and  $r = 2$  mm are shown in Fig. 14 and 15, respectively. The contribution of the components corresponding to the complex conjugate exponents  $\delta_1$  and  $\delta_2$  to the total mechanical stresses and displacements as well as the electric displacements and potential are equivalent. The stress, displacement and electric potential fields corresponding to the third exponent  $\delta_3$  are proportional to those of the first one  $\delta_1$  and the second one  $\delta_2$ , but its effect to the total fields is more significant for the electric displacements and electric potential only. However, the correspondence between the analytical and the FEM solution is very good for both radii  $r = 0.001$  mm and  $r = 2$  mm, respectively.

In the current research authors considered the poling only in coincidence with one of the Cartesian coordinate axis, mostly  $x_2$  or  $x_3$ . This fact follows from the manufacturing technology, operational purpose and relations for materials eigenvalues. But there are some situations that can cause an abrupt change of poling direction. When a body is subjected to the high compressive load in the direction of the spontaneous polarization or to the high tensile load perpendicular to the direction of the spontaneous polarization, the electric domain can switch by  $90^\circ$ . The polarization can be also switched by applying electric field with different direction, which can force the crystal to transform to one of the other five possible configurations. The extended LES formalism described above can provides solutions with arbitrary poling direction in the plane  $x_1 x_2$ .

350 The graphs in Figs. 16 and 17 show stresses, mechanical as well as electric displacements and electric potential for PZT-5H/PZT-4 bi-material notch defined by angles  $\omega_1 = 155^\circ$ ,  $\omega_2 = -180^\circ$ , where the poling of the PZT-5H is  $\alpha_1 = 40^\circ$ . We can again observe an excellent agreement between the numerical FEM solution and analytical description via the extended LES formalism.

## 355 8. Conclusion

The extended Lekhnitskii-Eshelby-Stroh formalism for piezoelectric materials was applied on bi-material notches and interface crack problem. Even that these two kinds of the stress concentrators are usually studied separately, especially in the case of the piezoelectric materials, the presented results showed that 360 the used form of the extended LES formalism covers acceptable both particular fields of the fracture mechanics. Additionally, the singularities of very closed bi-material notches, whose stress terms showing the complex valued exponents were part of the discussion. Also arbitrary poling orientation of the piezoelectric materials in the  $x_1x_2$  plane was included into the considerations. The generalization of the so-called  $\varepsilon$  and  $\kappa$  classification of the piezoelectric bi-materials 365 to the type A and B, respectively, was suggested. It was ascertained that the exponents of the singularity of the stresses, mechanical and electric displacements and electric potential are independent on the parallel poling orientation of the bi-material. Although in the case of the interface crack the used exponent eigenvalue procedure is not able to distinguish between the real and complex exponent form as do the Hilbert problem presented in Ou and Wu [36], it was shown that both methods give equivalent results. Finally the  $\Psi$ -integral method was used to GSIF evaluation for various piezoelectric bi-material and notch configurations. After an introduction of the improved numerical treatment caused 370 by the ill-conditioning of the matrices in the piezoelectric constitutive law, a very good approximation of all components of mechanical and electrical characteristics was shown as well as the  $\Psi$ -integral path-independence.

## Acknowledgements

?

## 380 Appendix A. FEniCS 2018.1 script for interface crack in piezoelectric bi-material

A FEniCS offers the way to solve numerically the weak formulation (21). The mesh of the domain  $\Omega$  has to be imported from any external mesh tool. An example of the model made in such tool (GMSH software [62]) of the interface crack, whose dimensions are given in Fig. 10, is shown in the Fig. A.18. The 385 physical tags of the subdomains and boundaries must be included in the mesh import to allow FEniCS to assign them the corresponding material characteristics and boundary conditions. The Neumann and Dirichlet boundary conditions

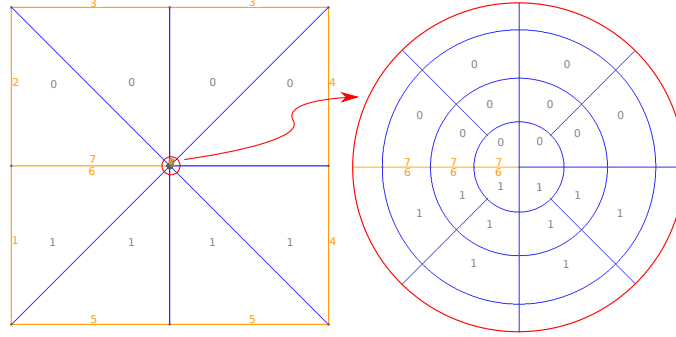


Figure A.18: The physical tags of the boundary and subdomains generated by GMSH mesh software.

(19) and (18) are prescribed according to the model in Fig. 10. More information about FEniCS can be found on the FEniCS project website [61] and in Logg et al. [51]. The FEniCS script written in Python is follows:

```

import os
#-----[FEniCS 2018.1]-----
from dolfin import *
395 #-----[ PZT-5H ]-----
#-----[stiffness >Pa<]-----
C0_11=11.7e10
C0_12=5.30e10
C0_23=5.50e10
400 C0_22=12.6e10
C0_44=3.53e10
C0_66=(C0_22-C0_23)/2
#-----[piezoelectric coefficients >C/m2<]-----
e0_12=-6.50
405 e0_11=23.30
e0_26=17.00
#-----[dielectric permittivity >10e-9 C/Vm<]-----
omega0_11=13.0e-9
omega0_22=15.1e-9
410 #-----[ BaTiO3 ]-----
#-----[stiffness >Pa<]-----
C1_11=14.6e10
C1_12=6.60e10
C1_23=6.60e10
415 C1_22=15.0e10
C1_44=4.40e10
C1_66=(C1_22-C1_23)/2
#-----[piezoelectric coefficients >C/m2<]-----

```

```

e1_12=-4.35
420 e1_11=17.50
e1_26=11.40
#-----[dielectric parmittivity >10e-9 C/Vm<]-----
omega1_11=11.2e-9
omega1_22=9.87e-9
425 #-----[mesh convert to FEniCS xml]-----
os.system("dolfin-convert bicrack0.msh bicrack0.xml")
#-----[mesh import]-----
mesh=Mesh('bicrack0.xml')
#-----[domain and boundary physical tags]-----
430 domains=MeshFunction("size_t",mesh,'bicrack0_physical_region.xml')
boundaries=MeshFunction("size_t",mesh,"bicrack0_facet_region.xml")
#-----[matrices of the constitutive laws]-----
C0=as_matrix([[C0_11,C0_12,0.],[C0_12,C0_22,0.],[0.,0.,C0_44]])
C1=as_matrix([[C1_11,C1_12,0.],[C1_12,C0_22,0.],[0.,0.,C1_44]])
435 e0=as_matrix([[e0_11,e0_12,0.],[0.,0.,e0_26]])
e1=as_matrix([[e1_11,e1_12,0.],[0.,0.,e1_26]])
omega0=as_matrix([[omega0_11,0.],[0.,omega0_22]])
omega1=as_matrix([[omega1_11,0.],[0.,omega0_22]])
#-----[constant definition]-----
440 null=Constant(0.)
#-----[piezoelectricity characteristic]-----
def eps(u):
    Du=grad(u)
    return 0.5*(Du + Du.T)
445 def E(phi):
    Ephi=-grad(phi)
    return Ephi
def strain2voigt(e):
    return as_vector([e[0,0],e[1,1],2*e[0,1]])
450 def voigt2stress(s):
    return as_tensor([[s[0],s[2]],[s[2],s[1]]])
def sigma0(u,phi):
    su=voigt2stress(dot(C0,strain2voigt(eps(u))))
    sphi=voigt2stress(dot(e0.T,E(phi)))
455 return su-sphi
def sigma1(u,phi):
    su=voigt2stress(dot(C1,strain2voigt(eps(u))))
    sphi=voigt2stress(dot(e1.T,E(phi)))
    return su-sphi
460 def D0(u,phi):
    Du=dot(e0,strain2voigt(eps(u)))
    Dphi=dot(omega0,E(phi))
    return Du+Dphi
def D1(u,phi):

```

```

465     Du=dot(e1,strain2voigt(eps(u)))
        Dphi=dot(omega1,E(phi))
        return Du+Dphi
#-----[measure symbols]-----
ds=Measure("ds",domain=mesh,subdomain_data=boundaries)
470 dx=Measure("dx",domain=mesh,subdomain_data=domains)
#-----[fixed point of boundary]-----
def pinpoint5(x,on_boundary):
    return near(x[0],0) and near(x[1],-90e-3)
#-----[external loading]-----
475 class tractions3(UserExpression):
    def eval(self,value,x):
        value[0]=0.
        value[1]=1.e4 # >Pa<
    def value_shape(self):
480         return (2,)
#-----[function spaces]-----
V=VectorElement("CG",mesh.ufl_cell(),2)
VV=FiniteElement("CG",mesh.ufl_cell(),2)
#-----[mixed function space]-----
485 MX=FunctionSpace(mesh,MixedElement([V,VV]))
#-----[Neumann boundary conditions]-----
tr3=tractions3(element=MX.ufl_element())
#-----[Dirichlet boundary conditions]-----
bcs=[DirichletBC(MX.sub(0).sub(0),null,pinpoint5,'pointwise'),
490      DirichletBC(MX.sub(0).sub(1),null,boundaries,5),
      DirichletBC(MX.sub(1),null,boundaries,5)]
#-----[trial and test functions]-----
(u,u_phi)=TrialFunctions(MX)
(w,w_phi)=TestFunctions(MX)
495 #-----[weak formulation - left hand side]-----
a1=-inner(sigma0(u,u_phi),eps(w))*dx(0)-inner(sigma1(u,u_phi),eps(w))*dx(1)
a2=inner(D0(u,u_phi),E(w_phi))*dx(0)+inner(D1(u,u_phi),E(w_phi))*dx(1)
a=a1+a2
#-----[weak formulation - right hand side]-----
500 l1=-tr3[0]*w[0]*ds(3)-tr3[1]*w[1]*ds(3)
l=l1
#-----[solution of weak formulation]-----
A,b=assemble_system(a,l,bcs,finalize_tensor=True)
solver=LUSolver(A,'default')
505 mx=Function(MX)
solver.solve(A,mx.vector(),b)
#-----[splitting weak solution to displacements and el.potential]-----
u_sol,phi_sol=mx.split()
#-----[stresses and el.displacements aproximation]-----
510 T_plot=TensorFunctionSpace(mesh,"CG",1,shape=(2,2))

```

```

s0=project(sigma0(u_sol,phi_sol),T_plot)
s1=project(sigma1(u_sol,phi_sol),T_plot)
D_plot=TensorFunctionSpace(mesh,"CG",1,shape=(2,))
d0=project(D0(u_sol,phi_sol),D_plot)
515 d1=project(D1(u_sol,phi_sol),D_plot)
#-----[result saving]-----
file1=File('bicrack1_u.pvd')
file1 << u_sol
file2=File('bicrack1_phi.pvd')
520 file2 << phi_sol
file3=File('bicrack1_s0.pvd')
file3 << s0
file4=File('bicrack1_s1.pvd')
file4 << s1
525 file5=File('bicrack1_d0.pvd')
file5 << d0
file6=File('bicrack1_d1.pvd')
file6 << d1

```

## References

- 530 [1] D. Barnett, J. Lothe, Dislocation and line charges in anisotropic piezo-electric insulators, *Physical Status Solidi (b)* 67 (1975) 105–111. doi:10.1002/pssb.2220670108.
- [2] Y. Pak, Crack Extension Force in a Piezoelectric Material, *Journal of Applied Mechanics* 57 (3) (1990) 647. doi:10.1115/1.2897071.
- 535 [3] C. Kuo, D. Barnett, Stress Singularities of Interfacial Cracks in Bonded Piezoelectric Half-Spaces, in: J. Wu, T. Ting, D. Barnett (Eds.), *Modern Theory of Anisotropic Elasticity and Applications*, Siam, Philadelphia, 1991, pp. 33–50.
- [4] Z. Suo, C. Kuo, D. Barnett, J. Willis, *Fracture Mechanics for Piezoelectric Ceramics*.Pdf (1992).
- 540 [5] S. Park, C. Sun, Effect of electric field on fracture of piezoelectric ceramics, *International Journal of Fracture* 70 (3) (1995) 203–216. doi:10.1007/BF00012935.  
URL <http://dx.doi.org/10.1007/BF00012935>
- 545 [6] Y. C. Liang, C. Hwu, Electromechanical analysis of defects in piezoelectric materials, *Smart Materials and Structures* 5 (3) (1996) 314–320. doi:10.1088/0964-1726/5/3/009.
- [7] M. Chung, T. Ting, Piezoelectric solid with an elliptic inclusion or hole, *International Journal of Solids and Structures* 33 (23) (1996) 3343–3361. doi:10.1016/0020-7683(95)00189-1.
- 550

URL <http://www.sciencedirect.com/science/article/pii/S0020768395001891>

- [8] H. Sosa, N. Khutoryansky, New developments concerning piezoelectric materials with defects, *International Journal of Solids and Structures* 33 (23) (1996) 3399–3414. doi:10.1016/0020-7683(95)00187-5.  
555 URL <http://www.sciencedirect.com/science/article/pii/S0020768395001875>
- [9] Z. C. Ou, Y. H. Chen, Explicit expressions of eigenvalues and eigenvectors for transversely isotropic piezoelectric materials, *Acta Mechanica* 162 (1-4) (2003) 213–219. doi:10.1007/s00707-002-1010-1.  
560
- [10] C. Hwu, Some explicit expressions of extended Stroh formalism for two-dimensional piezoelectric anisotropic elasticity, *International Journal of Solids and Structures* 45 (16) (2008) 4460–4473. doi:10.1016/j.ijsolstr.2008.03.025.
- [11] C. Hwu, T. Ikeda, Electromechanical fracture analysis for corners and cracks in piezoelectric materials, *International Journal of Solids and Structures* 45 (22-23) (2008) 5744–5764. doi:10.1016/j.ijsolstr.2008.06.011.  
565
- [12] C. Hwu, T. Kuo, Interface Cracks/Corners in Anisotropic/Piezoelectric materials, 3rd International Conference on Integrity, Reliability and Failure, Porto/Portugal 20-24 July 2009 (July) (2009) 20–24.  
570
- [13] C. Hwu, T. Kuo, Interface corners in piezoelectric materials 110 (April) (2010) 95–110. doi:10.1007/s00707-010-0318-5.
- [14] C. Hwu, *Anisotropic Elastic Plates*, 1st Edition, Springer US, 2010.
- [15] C. Hwu, A Unified Definition of Stress Intensity Factors for Cracks/Corners/Interface Cracks/Interface Corners in Anisotropic/Piezoelectric/Viscoelastic Materials, *Procedia Materials Science* 3 (2014) 257–263. doi:10.1016/j.mspro.2014.06.045.  
575 URL <http://linkinghub.elsevier.com/retrieve/pii/S2211812814000467>  
580
- [16] H. Hirai, M. Chiba, M. Abe, T. Ikeda, N. Miyazaki, Stress intensity factor analysis of an interfacial corner between piezoelectric bimaterials using the H-integral method, *Engineering Fracture Mechanics* 82 (2012) 60–72. doi:10.1016/j.engfracmech.2011.11.023.  
585 URL <http://dx.doi.org/10.1016/j.engfracmech.2011.11.023>
- [17] M. Abe, T. Ikeda, M. Koganemaru, N. Miyazaki, Stress intensity factor analysis of a three-dimensional interfacial corner between anisotropic piezoelectric multi-materials under several boundary conditions on the corner surfaces, *Engineering Fracture Mechanics* 171 (2017) 1–21. doi:

- 590 10.1016/j.engfracmech.2016.12.009.  
 URL <http://dx.doi.org/10.1016/j.engfracmech.2016.12.009>
- [18] L. Belokopytova, L. Fil'shtinskii, Two-dimensional boundary value problem of electroelasticity for a piezoelectric medium with cuts, *J. Appl. Math. Mech.* 43 (1979) 147–153.
- 595 [19] H. Sosa, Plane problems in piezoelectric media with elliptic inclusion, *Int. J. Solids Structures* 28 (4) (1991) 491–505. doi:10.1007/BF02457682.
- [20] T. Chen, D. Lai, An exact correspondence between plane piezoelectricity and generalized plane strain in elasticity, *Proc. R. Soc. Lond.* 453 (1997) 2689–2713.
- 600 [21] T. Chen, W. J. Yen, Piezoelectric analogy of generalized torsion in anisotropic elasticity, *Journal of Elasticity* 49 (3) (1997) 239–256. doi:10.1023/A:1007426225271.
- [22] T. Chen, Further correspondences between plane piezoelectricity and generalized plane strain in elasticity, *Proceedings of the Royal Society A: Mathematical, Physical and Engineering Sciences* 454 (1971) (1998) 873–884. doi:10.1098/rspa.1998.0190.  
 605 URL <http://rspa.royalsocietypublishing.org/cgi/doi/10.1098/rspa.1998.0190>
- [23] C.-F. Gao, J.-H. Yu, Two-dimensional analysis of a semi-infinite crack in piezoelectric media, *Mechanics Research Communications* 25 (6) (1998) 695–700. doi:10.1016/S0093-6413(98)00089-5.  
 610 URL <https://www.sciencedirect.com/science/article/pii/S0093641398000895>
- [24] X.-L. Xu, R. Rajapakse, Analytical solution for an arbitrarily oriented void/crack and fracture of piezoceramics, *Acta Materialia* 47 (6) (1999) 1735–1747. doi:10.1016/S1359-6454(99)00075-0.  
 615 URL <http://www.sciencedirect.com/science/article/pii/S1359645499000750>
- [25] Z. Huang, Z.-B. Kuang, Explicit expression of the A and B matrices for piezoelectric media, *Mechanics Research Communications* 27 (5) (2000) 575–581. doi:10.1016/S0093-6413(00)00132-4.  
 620 URL <https://www.sciencedirect.com/science/article/pii/S0093641300001324>
- [26] X.-L. Xu, R. Rajapakse, On singularities in composite piezoelectric wedges and junctions, *International Journal of Solids and Structures* 37 (23) (2000) 3253–3275. doi:10.1016/S0020-7683(99)00143-2.  
 625 URL <http://www.sciencedirect.com/science/article/pii/S0020768399001432>



- [27] C.-H. Chue, C.-D. Chen, Decoupled formulation of piezoelectric elasticity under generalized plane deformation and its application to wedge problems, *International Journal of Solids and Structures* 39 (12) (2002) 3131–3158. doi:10.1016/S0020-7683(02)00247-0.  
URL <https://www.sciencedirect.com/science/article/pii/S0020768302002470>
- [28] C.-D. Chen, On the singularities of the thermo-electro-elastic fields near the apex of a piezoelectric bonded wedge, *International Journal of Solids and Structures* 43 (5) (2006) 957–981. doi:10.1016/J.IJSOLSTR.2005.03.011.  
URL <https://www.sciencedirect.com/science/article/pii/S0020768305001228>
- [29] Z. Ou, Y. Chen, Near-tip stress fields and intensity factors for an interface crack in metal/piezoelectric bimaterials, *International Journal of Engineering Science* 42 (13-14) (2004) 1407–1438. doi:10.1016/J.IJENGSCI.2004.01.008.  
URL <https://www.sciencedirect.com/science/article/pii/S0020722504001065>
- [30] C. H. Xu, Z. H. Zhou, X. S. Xu, A. Y. Leung, Electroelastic singularities and intensity factors for an interface crack in piezoelectric-elastic bimaterials, *Applied Mathematical Modelling* 39 (9) (2015) 2721–2739. doi:10.1016/j.apm.2014.10.061.
- [31] T. Sasaki, T. Kondo, T. Tane, Analogy of Stress Singularities Analysis between Piezoelectric Materials and Anisotropic Materials, *Procedia Materials Science* 3 (2014) 1767–1772. doi:10.1016/J.MSPRO.2014.06.285.  
URL <https://www.sciencedirect.com/science/article/pii/S2211812814002867>
- [32] L. Banks-Sills, Y. Motola, L. Shemesh, The M-integral for calculating intensity factors of an impermeable crack in a piezoelectric material, *Engineering Fracture Mechanics* 75 (5) (2008) 901–925. doi:10.1016/j.engfracmech.2007.05.009.  
URL <http://www.sciencedirect.com/science/article/pii/S001379440700255X>
- [33] Z. Suo, Singularities, interfaces and cracks in dissimilar anisotropic media, *Proceedings of the Royal Society A: Mathematical, Physical and Engineering Sciences* doi:10.1098/rspa.1990.0016.
- [34] Q.-H. Qin, S.-W. Yu, An arbitrarily-oriented plane crack terminating at the interface between dissimilar piezoelectric materials, *International Journal of Solids and Structures* 34 (5) (1997) 581–590. doi:10.1016/S0020-7683(96)00040-6.  
URL <http://www.sciencedirect.com/science/article/pii/S0020768396000406>

- [35] W.-Y. Tian, Y.-H. Chen, Interaction between an interface crack and subinterface microcracks in metal/piezoelectric bimaterials, *International Journal of Solids and Structures* 37 (52) (2000) 7743–7757. doi:10.1016/S0020-7683(00)00110-4.  
 675 URL <https://www.sciencedirect.com/science/article/pii/S0020768300001104>
- [36] Z. Ou, X. Wu, On the crack-tip stress singularity of interfacial cracks in transversely isotropic piezoelectric bimaterials, *International Journal of Solids and Structures* 40 (26) (2003) 7499–7511. doi:10.1016/j.ijsolstr.2003.08.021.  
 680 URL <http://www.sciencedirect.com/science/article/pii/S0020768303004797>
- [37] Z. Ou, Y. Chen, Interface crack-tip generalized stress field and stress intensity factors in transversely isotropic piezoelectric bimaterials, *Mechanics Research Communications* 31 (4) (2004) 421–428. doi:10.1016/J.MECHRESCOM.2003.08.004.  
 685 URL <https://www.sciencedirect.com/science/article/pii/S0093641303001113>
- [38] Z. C. Ou, Y. H. Chen, Interface crack problem in elastic dielectric/piezoelectric bimaterials, *International Journal of Fracture* 130 (1) (2004) 427–454. doi:10.1023/B:FRAC.0000049502.54417.1c.  
 690
- [39] J. Sladek, V. Sladek, M. Wünsche, C. Zhang, Analysis of an interface crack between two dissimilar piezoelectric solids, *Engineering Fracture Mechanics* 89 (2012) 114–127. doi:10.1016/J.ENGFRACMECH.2012.04.032.  
 695 URL <https://www.sciencedirect.com/science/article/pii/S0013794412001774>
- [40] T. Ting, *Anisotropic Elasticity : Theory and Applications*, Oxford University Press, New York, 1996.
- [41] T. Profant, J. Klusák, O. Ševeček, M. Hrstka, M. Kotoul, An energetic criterion for a micro-crack of finite length initiated in orthotropic bi-material notches, *Engineering Fracture Mechanics* 110 (2013) 396–409. doi:10.1016/j.engfracmech.2013.08.014.  
 700
- [42] Y. Pak, Linear electro-elastic fracture mechanics of piezoelectric materials, *International Journal of Fracture* 54 (1) (1992) 79–100. doi:10.1007/BF00040857.  
 705
- [43] J. Nye, *Physical Properties of Crystals, Their Representation by Tensors and Matrices*, Oxford University Press, Oxford, 1985.
- [44] H. Fan, Decay Rates in a Piezoelectric Strip, *International Journal of Engineering Science* 33 (8) (1995) 1095–1103. doi:[https://doi.org/10.1016/0020-7225\(94\)00126-5](https://doi.org/10.1016/0020-7225(94)00126-5).  
 710

- [45] W. Zikung, Z. Bailin, The general solution of three-dimensional problems in piezoelectric media, *International Journal of Solids and Structures* 32 (1) (1995) 105–115. doi:10.1016/0020-7683(94)00101-2.
- [46] C. H. Chue, C. D. Chen, Antiplane stress singularities in a bonded bimaterial piezoelectric wedge, *Archive of Applied Mechanics (Ingenieur Archiv)* 72 (9) (2003) 673–685. doi:10.1007/s00419-002-0241-x.  
URL <http://link.springer.com/10.1007/s00419-002-0241-x>
- [47] C. D. Chen, C. H. Chue, Singular electro-mechanical fields near the apex of a piezoelectric bonded wedge under antiplane shear, *International Journal of Solids and Structures* 40 (23) (2003) 6513–6526. doi:10.1016/S0020-7683(03)00415-3.  
URL <https://www.sciencedirect.com/science/article/pii/S0020768303004153>
- [48] B. L. Wang, Y. G. Sun, Out-of-plane interface cracks in dissimilar piezoelectric materials, *Archive of Applied Mechanics* 74 (1-2) (2004) 2–15. doi:10.1007/s00419-003-0286-5.
- [49] C. Cheng, X. Cheng, Z. Niu, N. Recho, Singularity characteristic analyses for magneto-electro-elastic V-notches, *European Journal of Mechanics - A/Solids* 57 (2016) 59–70. doi:10.1016/J.EUROMECHSOL.2015.12.005.  
URL <https://www.sciencedirect.com/science/article/pii/S0997753815001679>
- [50] A. Benjeddou, Advances in piezoelectric finite element modeling of adaptive structural elements: a survey, *Computers and Structures* 76 (1) (2000) 347 – 363. doi:https://doi.org/10.1016/S0045-7949(99)00151-0.  
URL <http://www.sciencedirect.com/science/article/pii/S0045794999001510>
- [51] A. Logg, K.-A. Mardal, G. Wells, *Automated Solution of Differential Equations by the Finite Element Method*, Springer-Verlag Berlin Heidelberg, 2012. doi:10.1007/978-3-642-23099-8.
- [52] P. Ciarlet, *The Finite Element Method for Elliptic Problems*, *Studies in Mathematics and its Applications*, Elsevier Science, 1978.  
URL <https://books.google.cz/books?id=TpHfoXnpKvAC>
- [53] X. Wang, K. Zhou, Twelve-dimensional Stroh-like formalism for Kirchhoff anisotropic piezoelectric thin plates, *International Journal of Engineering Science* 71 (2013) 111–136. doi:10.1016/j.ijengsci.2013.06.004.  
URL <http://www.sciencedirect.com/science/article/pii/S002072251300089X>
- [54] R. Desmorat, F. Leckie, Singularities in bi-materials: parametric study of an isotropic/anisotropic joint, *European Journal of Mechanics - A/Solids* 17 (1) (1998) 33–52. doi:10.1016/S0997-7538(98)80062-4.

- [55] O. Ševeček, Solution of general stress concentrators in anisotropic media by combination of FEM and the complex potential theory, Doctoral thesis, Brno University of Technology (2009).
- 755 [56] P. J. Papadakis, I. Babuska, A numerical procedure for the determination of certain quantities related to the stress intensity factors in two-dimensional elasticity, *Computer Methods in Applied Mechanics and Engineering* 122 (1-2) (1995) 69–92. doi:10.1016/0045-7825(94)00748-C.
- 760 [57] G. B. Sinclair, M. Okajima, J. H. Griffin, Path independent integrals for computing stress intensity factors at sharp notches in elastic plates, *International Journal for Numerical Methods in Engineering* 20 (6) (1984) 999–1008. doi:10.1002/nme.1620200603.
- 765 [58] L. Vu-Quoc, V. X. Tran, Singularity analysis and fracture energy-release rate for composites: Piecewise homogeneous-anisotropic materials, *Computer Methods in Applied Mechanics and Engineering* 195 (37-40) (2006) 5162–5197. doi:10.1016/j.cma.2005.11.009.
- [59] I. Sokolnikoff, *Mathematical Theory of Elasticity*, Tata McGraw-Hill, New York, 1956.
- [60] ANSYS® Academic Research Mechanical, Release 18.1.
- 770 [61] FEniCS Project 2018.1.  
URL <https://fenicsproject.org>
- [62] GMSH - A three-dimensional finite element mesh generator with built-in pre- and post-processing facilities.  
URL [gmsh.info](http://gmsh.info)